NTNU

Norwegian University of
Science and Technology

Design of a Lab Setup for testing Stator Windings in Ironless Axial Flux Machines

Eirik Mathias Husum

Norwegian University of Science and Technology
Department of Electrical Power Engineering

Problem Description

An ironless axial flux dual rotor permanent magnet electrical machine is to be designed and built. The purpose of the machine shall be to test different types of windings, and the machine should therefore be made in such a way that the stator is easily changed.

Assignment given: 22. January 2008
Supervisor: Robert Nilssen, ELKRAFT

Design of a Lab Setup for testing Stator Windings in Ironless Axial Flux Machines

Master Student, Eirik Mathias Husum, Department of Electrical Power Engineering, NTNU

Abstract—Axial flux machines may give higher power-to-weight ratios than conventional radial flux machines. As the axial flux machine can easily be constructed with a multi-rotor configuration, it is well suited for ironless stator design, which has gained interest in the latest years due to the development of high remanent flux density permanent magnets. In addition to the reduced eddy current losses and weight of the stator itself, an ironless design eliminates the magnetic forces acting on the stator, so that the necessity of a heavy stator frame is reduced.

Several winding topologies exists for ironless stators, and it can be interesting to compare these with each other. For this purpose, an ironless axial flux 110 pole dual rotor permanent magnet machine with easily exchangeable stator has been made. This machine allows preliminary tests on different stator designs before more expensive prototypes are built. As all active parts of the machine are visible, it may also serve as a demonstration model for electro-mechanical energy conversion.

Simulations done on a single-layer 3-level-endturn winding with q=6/5 shows an induced voltage of 40.22 V at 50 Hz. This corresponds well with measurements done on a stator segment covering 2/11 of the machine. The measured DC resistance of this segment is equivalent of 2.51 Ω for a complete stator, which even though somewhat less than calculated, is rather large due to long endturns compared to the radial length of the conductors. The measured inductance of the segment equals self and mutual inductances of about 0.55 μH and 0.275 μH for a complete stator, which is significantly less than calculated.

Index Terms—Ironless, winding, axial flux, permanent magnet, dual rotor.

I. Introduction

Most electrical synchronous machines are today made with a stator core of iron, as this reduces the reluctance for the rotor flux and thereby creates a stronger air gap flux. Due to the alternating current in the stator windings, eddy currents with appurtenant losses will be induced in the stator core. There will also be magnetic forces acting on the iron core. This is especially a problem in low-speed/large diameter axial flux machine, where the tolerance value for the stator position is extremely small compared to the stator diameter, as even small relative forces could cause the stator to touch the rotor. A robust frame for the stator is therefore needed, which in addition to the stator steel itself may constitute a considerable share of the machine's weight.

Electrical machines traditionally have been used in stationary applications, where weight is not a major issue. They are now however entering new fields such as propulsion systems in vehicles and wind turbines, with high requirements with respect to efficiency and/or weight. With the development of high remanent flux density permanent magnets, the stator may be made without iron core while still maintaining a reasonable air gap flux. Although the power output is somewhat decreased, the benefits of the reduced weight and increased efficiency may, in addition to the eliminated forces acting on the stator, compensate for this. As explained in section III, axial flux machines are well suited for ironless stator design.

The design of the machine presented in this paper started as a part of a master specialization project at NTNU [1], where it would take place in an ocean wave energy converter [2]. However, with a high pole number and inner-to-outer-diameter ratio close to unity, the machine had a design similar to what may be interesting for other applications, for instance direct driven wind turbines.

As ironless axial flux machines are a rather new concept, a lot of knowledge is yet to be found regarding different types of stator windings. The machine presented in this paper is meant to be an experimental setup allowing different kinds of windings to be used, so the impact these have on the machines performance can be studied before more expensive prototypes are being built.

II. Axial Flux Machines

Although the earliest known electrical machine, Faraday's disk generator developed in 1831 [3], was of the axial flux type, the market of electrical machines have more or less been dominated by radial flux machines since Davenport invented this in 1834 [4]. There may be several reasons for this: In a radial flux machine, the magnetic radial forces between the rotor and stator balances around the machine's circumference, while for an axial machine there will be a net axial force between the these. There are also high cost and difficulties involved in making laminated cores for axial machines: Since the laminates must be stacked in the radial direction in the axial machine, in contrast to the axial stacking of a radial machine, each layer will differ from the others. Finally, there may be problems involved in assembling the machine and keeping the axial airgap uniform [5].

The power of an electrical machine depends among other things heavily on the air gap area, as more area gives more flux linkage. A radial flux machine has an airgap area shaped as a cylinder surface, so that the airgap area is proportional with the machine's radius and axial length. The volume for radii inside the airgap does not contribute to the machine's power. The airgap of an axial flux machine is disk shaped, so the airgap area increases by the square of the machines radius. Even though the axial flux machine's airgap area is not depending on the axial length, one may increase the total airgap area by stacking several machines onto the same shaft. In theory, one may also stack several radial flux machines

with varying radii outside each other. However, this is a quite difficult task construction-wise, and no examples of such multi airgap radial machines are found in the literature. Based on this, the axial flux machine is likely to have a higher power density than radial machines [6].

Axial flux machines may also have other benefits besides a increased power density: The large diameters enables a high pole number, making it perfect for high torque/low speed operation, typical for direct driven devices. The large diameter to length ratio also makes the geometry suitable for applications like in-wheel-motors [7], wind turbines [8] and winches integrated in ship decks among others. As pointed out above, a modular approach may be used in the production: By stacking a different number of machines on the same shaft, a more or less the similar design may be used for different power levels. As the housing contribute significantly to the axial length of the machine, adding more modules in the axial direction will not necessarily increase the total axial length of the machine that much. Contrary, stacking n radial machines on the same shaft will increase the axial length by factor n, as the housing constitutes a minor share of the radial machines axial length.

III. IRONLESS STATOR SYNCHRONOUS MACHINES

Synchronous electrical machines may be made without a stator core. For a single-rotor-single-stator design without any return iron, the relative leakage flux will in that casae be significant, and a large amount of PM material is required in order to establish an adequate magnetic flux density through the windings. A RFPM machine of this configuration is presented in [9], having an flux density of 0.25 T at the windings. By introducing a rotating back iron or a second rotor, the airgap flux density will typically be in the range of 0.4-0.6 T. An example of a RFPM machine with ironless stator and rotating return iron is presented in [10]. By using a modular n-stator/$n+1$-rotor design, the stator coils are positioned between two facing poles, and the rotor iron may be omitted for all rotors except of the two outer ones. As discussed above, the AFPM is favored for such multi-rotor designs, making it preferable for ironless stator machines.

The absence of the stator iron reduces the weight of the machine, and the magnetic forces acting on the stator will more or less be eliminated, so that the mechanical structure may be simplified. There will nor be any reluctance variations for the rotor flux while this is rotating, so that the cogging force is dramatically reduced. The eddy-current losses normally found in stator cores are also removed in a coreless design, increasing the machine's efficiency. However, the flux passes the stator straight through the conductors in an ironless machine, instead of the teeth found in a slotted machine. The conductors will therefore experience the skin-depth effect, increasing the winding losses [11]. Also, the reluctance for the rotor flux is increased, so that the flux density in the stator is reduced. A coreless design therefore depends on a stronger magnetization, either by increased current in wound-field machines, or more or stronger PM-material in PM machines. One may also experience cooling problems, as the epoxy normally used in ironless stators has a lower heat conductivity compared to steel. It may therefore be necessary to include a cooling duct close to the stator windings [12].

IV. WINDING TOPOLOGIES FOR IRONLESS AFPMS

The main purpose of the machine presented in this paper is to test and compare different winding topologies for axial flux machines. There are several different topologies existing, each with their advantages and disadvantages.

A. Coil shapes

In order to achieve maximum flux linkage, the coils should be trapezoidal shaped, so that they cover the same angular length at the inner and the outer radius of the machine. This will however result in large endturns, increasing resistive losses and the non-active copper amount in the machine. For machines with an inner/outer airgap radius ratio close to unity and a high number of coils, the trapezoidal shape will approach a rectangular shape. By using rhomboidal coils, the endturn and their disadvantages may be eliminated. This will however be at the cost of reduce flux linkage, as the coil's area is reduced. A compromise is to use hexagonal coils, which both trapezoidal and rhomboidal coils are a type of, with angle β in Figure 1 being 0 and $\tau_c/2$ degrees respectively. These three shapes are, in addition to a circular shape coil, evaluated by [13]. Their FEM analysis shows that rhomboidal windings may give the same torque output as trapezoidal windings if the maximum allowed ohmic heat losses are kept the same, while hexagonal windings may give a torque 5% higher, both giving the benefit of reduced copper amount in the machine.
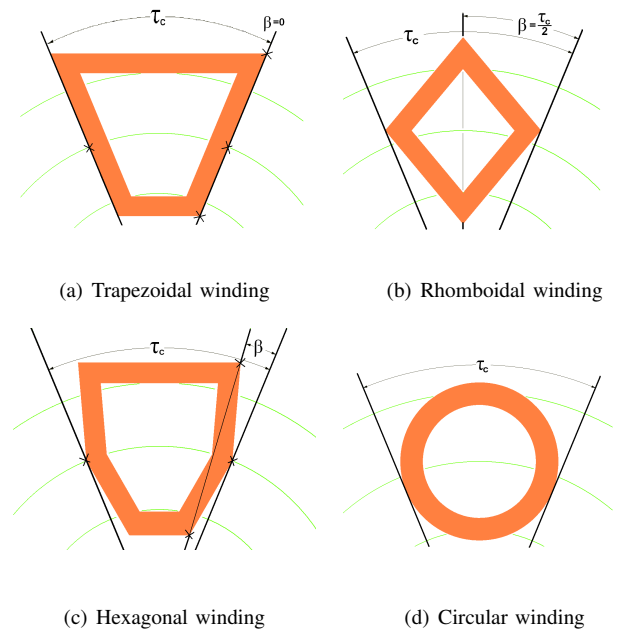

(a) Trapezoidal winding	(b) Rhomboidal winding
(c) Hexagonal winding	(d) Circular winding

Fig. 1.   Coil shapes. Note that both (a) and (b) is a type of (c), with $\beta = 0$ $\beta = \frac{\tau_c}{2}$ respectively.

B. Winding layout

1) Non-overlapping windings: In non-overlapping wind-ings, the coils are put side by side in the same plane as shown in Figure 2. The advantage of this is reduced end turns in the windings, as well as an easy assembly, as the coils don't need any deformation. The most basic type of this has 1 coil per phase per pole pair, with the outer edge of each coil spanning $\tau_c = \frac{2 \cdot \pi}{3}$ electrical rads, or a coil pitch of $\frac{2}{3}$ relative to the pole pitch of π rads.

Neglecting the inner distance in the coils, and also the distance from one coil to the next, so that the entire stator is filled with copper, the winding factor as a function of the coil pitch in electrical radians is in [14] described as

$$W = W_{fb} \cdot W_{fp} = \frac{4}{\tau_c} \sin^2 \frac{\tau_c}{4} \qquad (1)$$

Using $\tau_c = \frac{2 \cdot \pi}{3}$ gives a rather poor winding factor of 0.477.

By increasing the coil span to $\tau_c = \frac{4 \cdot \pi}{3}$ electrical rads, so that q=1/2, the winding factor is increased to 0.716, but at the cost of longer endturns [14]. The maximum theoreti-cal winding factor for concentrated windings is 0.7246, for $\tau_c = 1.484\pi$ resulting in a q = 0.4492. Although the fractions q=8/18, q=10/22 and q=18/40 would all result in a winding factor near this optimum, they would also experience a voltage loss as the coils within in each phase are not perfectly in phase with each other, so that the total voltage in the machine will be less than for q=1/2.

For so-called phase-grouped windings [15] all the coils of one phase are put next to each other, covering about 1/3 of the machine circumference, as shown in 3. Each coil then, depending on the number of poles and coils, covers roughly π electrical rads, giving a fairly good winding factor.

C. Overlapping windings

In a stator with overlapping windings, at least parts of the endturns must be stacked axially. In order to reduce the airgap length, the active part of the windings is normally placed in the same plane, meaning that axial part of the winding geometry is non-constant. This makes the overlapping windings a bit more complicated to produce than the non-overlapping ones. Also, the end turns will be longer.

A single layer overlapping 2-level-endturn layout is shown in Figure 4, with the endturns at two levels, alternating bent up and down [16]. This way, the endturns go around the entire stator.

A different layout for overlapping windings is the 3-level-endturn, where the coils are put together together in groups of three, as shown in Figure 5. Here the first coils endturn is bent down, the second flat, while the third one is bent up. Between two such groups, there are no endturns, making it possible to split the stator at this position without affecting the coils.

The overlapping winding may also have two levels of conductors in the airgap, making it similar to a two layer winding. A wave winding of this type may easily be produced by winding conductors onto a ring, as shown in Figure 6. Note that for this configuration, there are no closed coils on every pole, but a winding that makes it way back and forth between
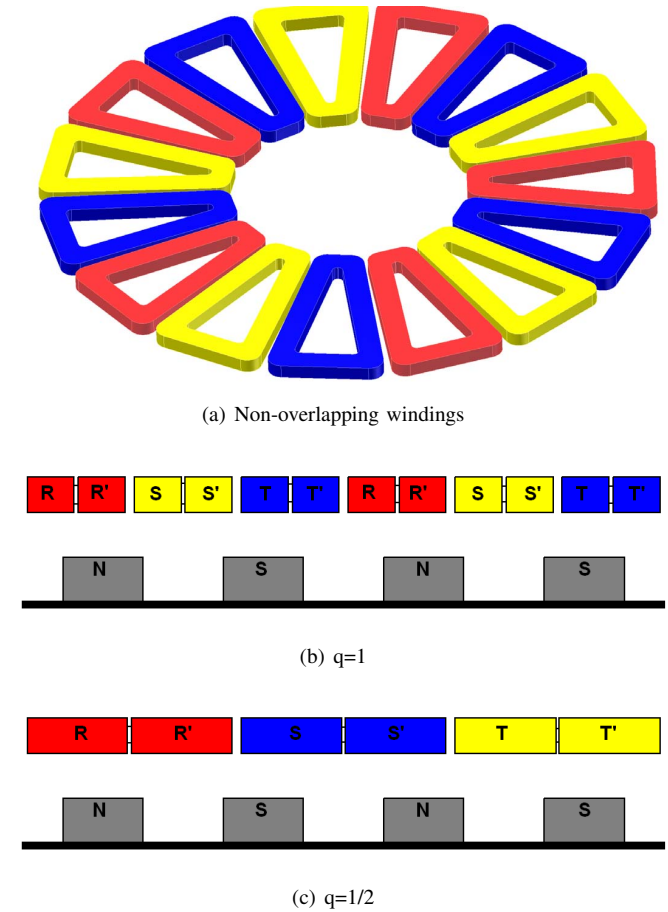

(a) Non-overlapping windings

(b) q=1

(c) q=1/2

Fig. 2.   Examples of non-overlapping winding layout, with q=1 and q=1/2.

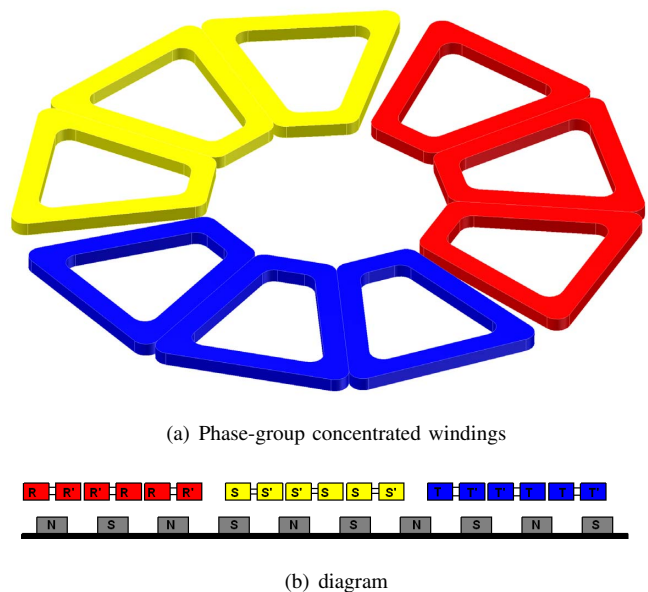

(a) Phase-group concentrated windings
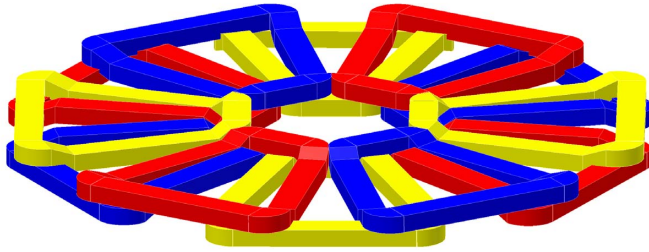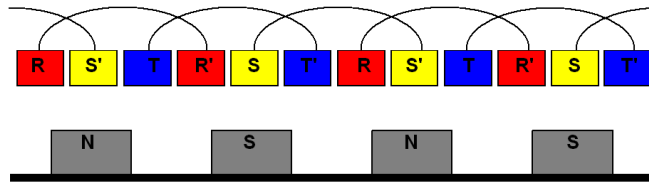

(b) diagram

Fig. 3.   Examples of phase-group concentrated winding layout for a machine with 10 poles.
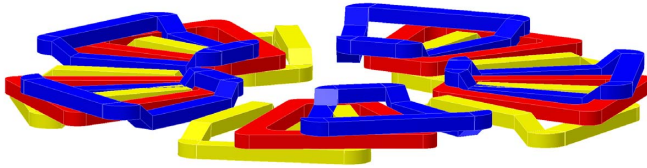
than iron.

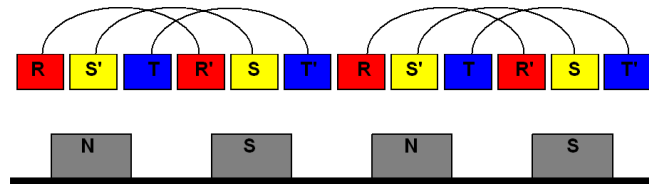(a) Overlapping 2-level-endturn windings

(b) diagram

Fig. 4.   Overlapping windings with 2-level-endturn.

(a) Overlapping 3-level-endturn windings

(b) diagram

Fig. 5.   Overlapping windings with 3-level-endturn.

the inner to the outer radius of the machine. A drawback is the increased airgap, while a benefit is the possibility of doubling the amount of active copper in the machine. By consequently putting the turn and return conductors on each own side of the ring, each coils side spans 120 degrees. [12] describes an ironless AFPM machine where the stator consists of rhomboidal shaped coils tread on a hollow ring. The interior of the ring is used for cooling the stator, which can be troublesome for large ironless machines, as the epoxy normally used in ironless machines has a lower thermal conductivity
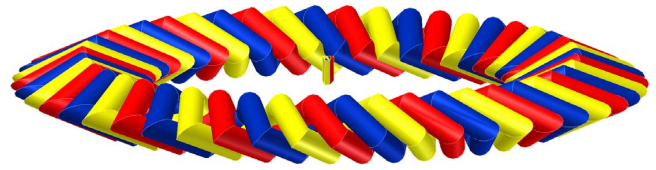
(a) Toroidal wound two layer wave winding. Note that each phase may carry several conductors in series, put side by side of each other, so that each phase has a 120° grouping
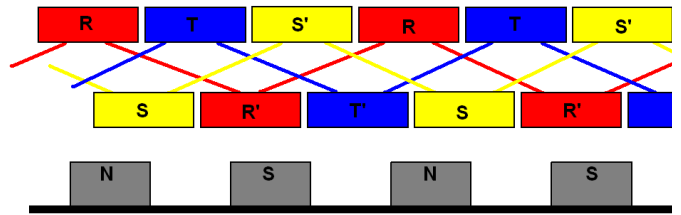
(b) diagram

Fig. 6.   Toroidal winding layout.

V. DESIGN

A. Criteria for q

The machine is easiest evaluated if its considered to consist of six phases, that is three phases, each with a turn and return component. The stator has of groups of three and three coils together, where one group always contains each of the six phases, always in the same sequence. However, the phase that starts the group may be changed. That gives six different groups:

1) R - S' - T - R' - S - T'
2) T' - R - S' - T - R' - S
3) S - T' - R - S' - T - R'
4) R' - S - T' - R - S' - T
5) T - R' - S - T' - R - S'
6) S' - T - R' - S - T' - R

In order to get a balanced system, each of these groups should be present the same number of times in the machine (the exception is if only one of the groups are used, as that would yield a non-fractional winding layout with q=1). That gives the first criterion for the machine:

$$n_{sp} = 6 \cdot k \qquad (2)$$

, where n_{sp} is the number of coil sides (equivalent to the slots in an slotted machine) per phase and k is an integer.

Further, each of the phases should spread no more than a sector of 60°. That involves for instance a S-coil side being normally succeeded by a T'-coil side. The exception is if the S-coil side is located in the first possible position of the sector,

as it then will still be room for another S-coil side in the sector. If so happens, one are changing from using group 2 to group 3. The consequence of all this is that a group i will either be succeeded by another group i, or a group $i + 1$. As the group number is increasing, a phase is gradually moving from front to the end of the group, before it jumps back to the beginning of the group. In order to maintain the 60° sector for each phase, the pole pitch must therefore be somewhat larger than the coil pitch. If the simplest group sequence, [1 2 3 4 5 6], is used, phase R appears six times. But as phase R in the last group is succeeded by a phase R in the first group, these must be within the same 60°, and thereby under the same pole pair. Therefore, the pole pair number must be a multiple of five, giving the machine a multiple of ten poles. This yields a q of $q = 36coil\ sides/10poles/6phases = 6/5$. If the second simplest group sequence, [1 1 2 2 3 3 4 4 5 5 6 6], is used, phase R appears twelve times. The pole pair number should then be twelve, giving a q of $q = 72coil\ sides/22poles/6phases = 12/11$. This results in the second criterion of the machine,

$$q = \frac{n_{sp}}{n_{sp} - 1} \tag{3}$$

Combining criterion (2) and (3) results in the fraction

$$q = \frac{i \cdot 6}{i \cdot 6 - 1} \tag{4}$$

, where i is an integer. As q is the number of slots per pole per phase, the pole number of the machine must be

$$p = (i \cdot 6 - 1) \cdot 2j \tag{5}$$

, where j is an integer.

A winding layout for a machine with q=6/5 is presented in Table I. Note that the phase direction is changed for every pole, so that coil side 4 in the R-sector under pole 2 is of the R'-phase; coil side 5 is S-phase, while coil side 6 and 7 is T'-phase etc.

TABLE I
WINDING LAYOUT FOR Q=6/5.

| R | | | | | | S' | | | | | | T | | | | | | |
0°	10°	20°	30°	40°	50°	60°	70°	80°	90°	100°	110°	120°	130°	140°	150°	160°	170°	°electrical
36					1						2					3		pole 1
			4					5					6				7	pole 2
				8					9					10				pole 3
	11					12					13				14			pole 4
			15					16					17					pole 5
18					19					20					21			pole 6
	22					23					24					25		pole 7
			26					27					28					pole 8
29					30					31					32			pole 9
			33					34					35					pole 10

As the one of the purposes of the machine is to test out stators with different winding configurations (but with the same pole number on the rotor), one should have a set of i that combined with a suitable j results in a constant pole number in (5). Disregarding $q = 1$, there are only two solutions that gives a reasonable pole number for the geometry used, with $q = \frac{6}{5}$ and $q = \frac{12}{11}$. The coincident pole number is then $p = 110$. The machine is therefore designed with a pole number of $p = 110$ and three different stators; with q=1, q=12/11 and q=6/5, where the q=12/11 and q=6/5 have electrical symmetry for every 12 and 6 groups respectively.

VI. CONSTRUCTION

A. Rotor

A 110 pole dual rotor ironless stator AFPM machine test rig has been constructed. The two rotors are mounted on a shared aluminum ring, connected by spokes to the central shaft of the machine. Each of the rotors consists of a 5 mm thick steel ring with inner and outer diameters of 640 mm and 740 mm. Using Locktite 326, 110 NeFeB magnets with dimensions 20mm x 10mm x 5mm and magnetization passing through biggest surface, are glued with the 10 mm side tangential to the outer edge of the ring, as shown in Figure 7(a) and Figure 7(c). That way the steel ring serves as a back iron for the rotor while also attaching the rotor to the aluminum ring. One should note the the weight of the rotors could have been decreased significantly by using steel rings that covers only the active part of the machine in the radial direction; at the current design the ring spans 50 mm in the radial direction, while the magnets span only 20 mm. One could also have reduced the thickness of the rings; in this design the rings' thickness is equivalent to half of the the magnet pitch, so that cross section average flux density in the ring is the same as on the magnet surface, far below magnetic saturation of the steel. However, reducing the size of the steel rings would have introduced the need for a support disk for the rotor, both in order to stabilize it the axial direction and for attaching it to the aluminum ring.

(a) Rotor ring (b) Magnet mould
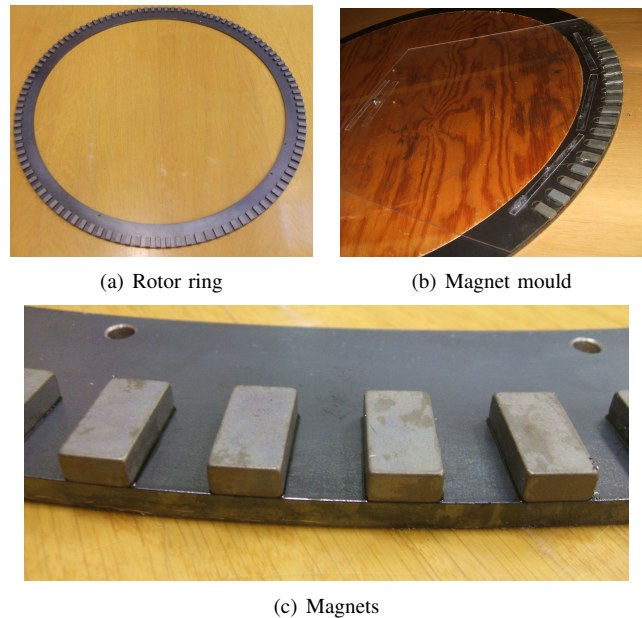

(c) Magnets

Fig. 7. Rotor

In order to maintain accuracy when mounting the magnets, a mould was cut out of a plastic plate, with space for 18 magnets, as shown in 7(b). The mould was centered in the steel ring, so that the slots could cover the entire ring at a constant radius. Due to the high pole number, and the need of moving the mould around the circumference, any error in the distance from one slot to another would propagate heavily. It therefore took four attempts before a mould accurate enough was produced. Even though the resolution of the drill was 0.005 mm, rotating

the plate a fixed distance between the cutting of each slot resulted in an error, that propagated when moving around the entire circumference. The position of each slot relative to a reference slot was therefore necessary when cutting the slots. To ensure that the mould was of sufficient accuracy, magnets without glue were put in the two outer slots, using these as a reference when moving the mould around the ring, and ensuring that the first magnet fitted into the mould after one revolution. This was also done when finally gluing the magnets, so that the mould was kept in place by two already glued magnets in each position. The slots were cut to fit the magnets exactly in the tangential direction. As more and more of the slot were filled up with magnets, the mould became tighter and tighter, and it was therefore somewhat problematic to insert the last magnets, as well as difficult to loosen the mould after gluing. Therefore, the slots were expanded some in the tangential direction by using a file, which may have caused some inaccuracy. For the second ring, some deviation may, for unknown reason, have occurred when gluing the last magnet section, as the mould didn't fit the magnets exactly.

Four spacers, each spreading about 10 cm in the tangential direction, where bolted onto the bicycle rim in order to attach the rotor rings and to keep these apart from each other. It proved that these spacers were not sufficient: When trying to mount the rings onto the aluminum ring, the magnetic attraction between the rings caused these to bend, so that they collapsed into each other at two positions and was pushed 5 cm away from each other at two others, as shown in Figure 8.

Fig. 8. Collapsed rotor. The magnets touch each other at the left front and right back of the picture, and are pushed 5 cm away from each other at the right front and left back.

Luckily, after the rings were separated, they restored their original shape. To provide more support, twelve more spacers were placed between the rings. The aluminum ring is connected to the rotating part of a two-sided repulsive axial magnetic bearing, constructed as a part of a master specialization project work perfromed at NTNU and founded by SmartMotor in 2006 [17]. One can argue the need for such a high performance bearing in a test setup like this. However, the machine presented in this paper was originally supposed to be a part of an ocean wave energy converter [2], presented by professor Robert Nilssen at NTNU, with unbalanced axial forces on the rotor.

B. Stator coils

Determined by the magnet size, the active part of the machine has an inner diameter of $D_{inner} = 700$ mm and an outer diameter $D_{outer} = 740$ mm. The stator consists of rectangular shaped copper coils glued between two plates made of Lexan, a thermoplastic material. The coils, shown in Figure 9(a) use circular shaped wire with diameter 1 mm, and have 20 turns, 5 in the axial direction and 4 in the tangential direction of the machine. The inner radial length of the coils is 30 mm, 10 mm longer than the radial length of the air gap, in order to allow some deformation when squeezing the windings (see below). The inner tangential designed width for coils of the three different stators is 16.56 mm, 14.85 mm and 13.14 mm.

(a) Single Coil   (b) Framework for squeezing

(c) Three coils in framework before deformation   (d) Three coils in framework after deformation, seen from the side

(e) Three coils in framework before deformation, seen from the front   (f) Deformed group of coils
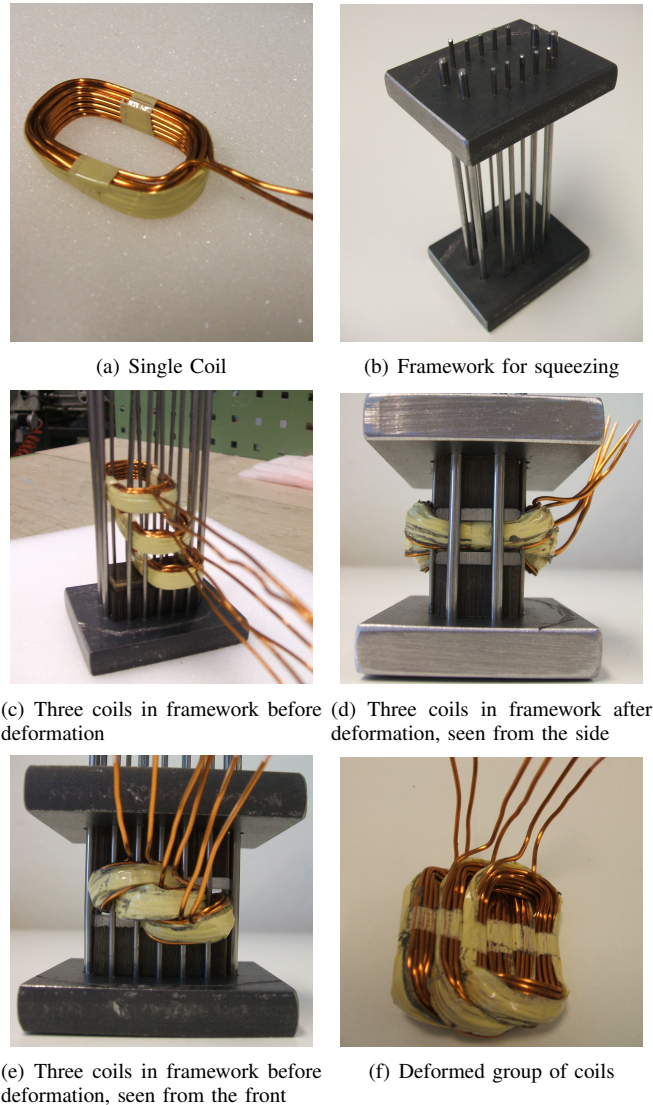
Fig. 9. Deformation of coils.

The windings are put in the machine in groups of three and three, with three level endturns. In order to keep the airgap as small as possible, the coils within a group are squeezed together, so that the active parts of all windings are in the same plane. To ensure that the windings geometry in the tangential direction is unaffected, the windings are put in a framework during the deformation, shown in Figure 7(b).

After deformation, the insulation between the phases were tested using a 500 V megaohm meter. In order to examine whether there were any damage within a coil, the inductance for each coil were measured using a LCR-meter, assuming that a coil with a short circuit between two turns would give a different value than a healthy one. All coils passed both of these tests. In order to check the validity of the tests, one coil group were damaged using a hammer and a screwdriver. The coils withstood a lot of damage before any different results were seen on the tests, which may indicate that some mildly damaged coils may have passed the tests. Still, if so, these coils should still work satisfactory in the machine, as the electrical parameters are unchanged.

C. Stator assembly

Using Loctite Hysol 9550, the windings are then glued between two 2 mm plates of Lexan, as shown in Figure 10(a). Some areas of the plates are removed, leaving space for the end windings, as well as enabling the coils of one group to be connected to the ones of the next group. In addition, a hole is drilled for each group, so that two rods from the framework can be used to position the groups on the plate. In addition to the coils, a sector of a 5 mm Lexan is glued between the two plates, providing mechanical support at the outer radius.
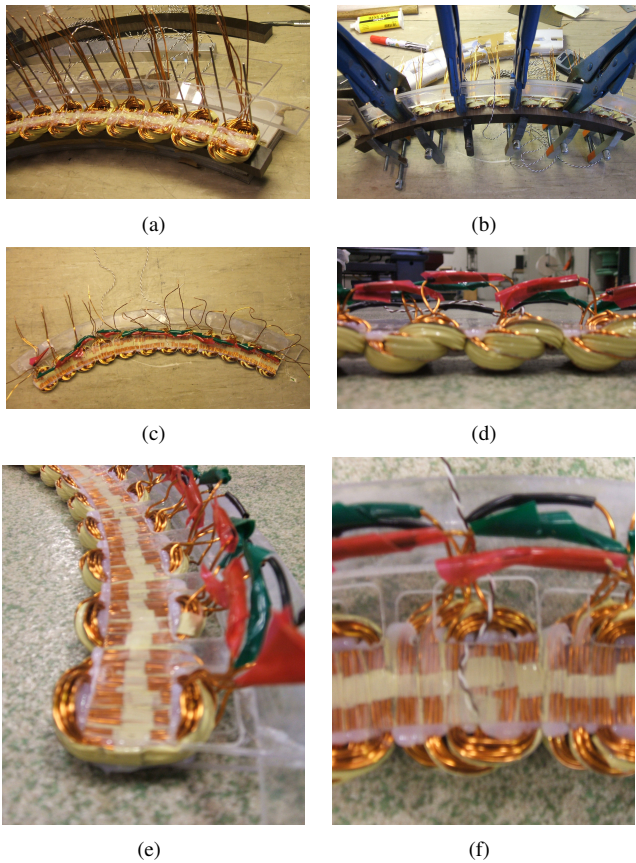

(a)	(b)
(c)	(d)
(e)	(f)

Fig. 10.   Assembly of a stator segment

For the stator with q=1, there will be 5 such sections containing 10 groups, plus one section with 5 groups. The stator with q=12/11 will have 5 sections of 12 groups, while the stator with q=6/5 has 5 sections of 12 groups plus one section with 6 groups. As discussed in V-A, the stator with q=12/11 is symmetrical for every 12 group, while the stator with q=6/5 is symmetrical for every 6 group. That means that any of the sections can be run alone, and still provide electrical symmetry. At the moment, only one segment of q=6/5 is made.

After the stator segment were glued together, it was noticed that one of coils had an open circuit. By visual inspection, it was found that the conductor was torn off just beneath the edge of the Lexan plate, as shown in Figure 11(a). It is assumed that this was caused by the pressure applied when gluing the coils between the plates, and the fact that the coils did not shape perfectly when during the deformation, as explained in VI-E. Luckily, as the damage was in one of the upper turns of the coil, it was possible to cut away a small piece of the Lexan plate, and solder the two conductor ends together. The tin solder was sprayed with insulating laquer, and the hole in the Lexan plate was filled with epoxy.

D. Stator frame

An important criterion for the machine is that it should be easy to change stator, so that different types of windings can be compared. Two concentric wooden rings, shown in Figure 11(d), one with diameters of 770 mm and 790 mm, the other with diameters 800 mm and 820 mm, provide support for the stator. The original idea was to have adjustments bolts on each stator segment that fitted between these rings, so that the stator's axial position could easily be controlled. These adjustment bolts should fit the gap between the concentric rings, so that the stator segment would be fixed in the radial direction, while the bolts is not fixed to a specific tangential position, as shown in Figure 11(c). This freedom in the tangential direction will make it easy to use other stator segments with different sizes later on. Because of lack of time, the segment were clamped onto the rings instead of using adjustment bolts, as shown in Figure 11(b). The rings are screwed onto four plates, that are adjustable in the axial direction, so that the windings can be positioned at the center of the airgap.

The axial length of the endturns is larger than the airgap between the two rotors. However, the rotor rings proved to be so flexible that they could be bent away from each other, leaving space for a stator segment to be inserted.

E. Comments on the mechanical design

The rotor rings are not completely flat: While the air gap distance seems to be rather constant, a small dip of maybe 0.5 mm can be seen on both rings when they are rotating. This increases the necessary mechanical clearing between the stator and the rotor rings. The dip may be caused by the collapse of the rotor rings or by the bending of the rings when inserting the stator segments, but it may also happen that the spacers connecting the rings to aluminum ring are positioned in different axial positions on the alumninum ring.

It was assumed that the center coil of each group would not be affected by the squeezing, and that this coil's endturn would not interact with the Lexan plate. This was not the

(a) Repair of damaged coil

(b) Stator segment clamped onto the stator frame

(c) Proposed screws for adjusting the stator segments in the axial direction

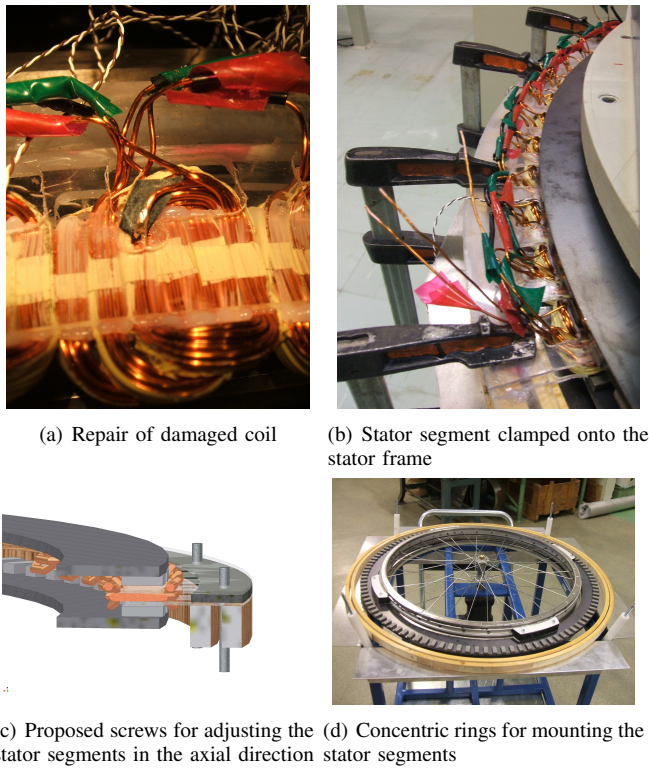(d) Concentric rings for mounting the stator segments

Fig. 11.

reality, and the result was that the Lexan plate deformed a little when they were glued and pressed together with the coil groups, so the axial length of the stator segment became a bit larger than predicted. This could have been avoided by putting a additional spacer for the conflicting endturn in the framework during the deformation.

In the current design, the coils are squeezed together so that they are flat for 20 mm, which is the length of the magnets in the radial direction. The magnets radial position varies to some extent, this is almost not visible, but may be felt by by running a finger along the ring's circumference. This makes it more likely that some magnets touch the coils. It proved to be difficult to position this flat section of the coils perfect relative to the magnets, and it could therefore have been an idea to extend the flat section of the windings a couple of millimeters. This can probably be done without altering the coil design, as it seems to be more than enough space at the endturns for the deformation.

As mentioned above, adjustment bolts should be used to connect the stator segments to the stator frame. It also seems as if the stator frame is not well enough positioned, or that the wooden rings are to flexible in the radial direction. This is not a problem as long as the stator segments are clamped onto these rings, but if the adjustment bolts are used, the result could be that the stator segment is fixed in a wrong radial position.

At the moment there is some touching between the stator and rotor when running the machine, both with magnets sweeping the Lexan plates, but also magnets hitting the endturns. This happens at certain positions on the rotor and stator, indicating that these are not as flat as they should be.

This problem can be reduced by adjusting the stator frame rings and the tightness of the clamps attaching the stator, but due to vibrations, it is impossible to keep the stator in a totally fixed position. The rotor has an eccentricity, causing the entire rig to swing at frequencies above 150 Hz.

VII. SIMULATIONS ON THE DESIGN

A. The influence of the relative magnet pitch

The energy is transferred between the rotor and stator as magnetic energy in the air gap. At any instant this energy is given as

$$W_{magn} = \frac{1}{2} \int_V \overrightarrow{B} \cdot \overrightarrow{H} \mathrm{d}V \qquad (6)$$

In order to have a high energy transfer, the air gap flux density should be as high as possible. This can be done by filling up the entire rotor surface with magnets. However, this increases the weight and material cost of the machine. In addition, increasing the magnet pitch will reduce the distance between two neighboring magnets, giving more leakage flux. At small air gaps, the flux distribution will also become more square-shaped, which leads to a high THD. On the other hand; having a small magnet pitch at large air gaps may lead to an almost triangular shaped flux distribution.

Using FEM, the flux distribution of a pole is analyzed for different magnet pitches. The simulations are done on an ironless axial flux dual rotor design with a pole pitch of 20 mm and magnet and back iron thickness of 5 mm. Three different total air gap lengths, including stator, are considered, 2.5 mm, 5 mm and 10 mm.

As the relative magnet pitch increases, so does the relative leakage flux, as shown in Figure 13. This is particularly valid for a 10 mm air gap. Because of that, the total effective air gap flux does, as shown in Figure 12, not increase linearly with the relative magnet pitch. That means that the W/kg magnet decreases as the relative magnet pitch increases, turning the relative magnet pitch into a power/weight or a power/cost optimization. In literature, the typical relative magnet pitch is found to be in the range 0.7-0.8 [16]
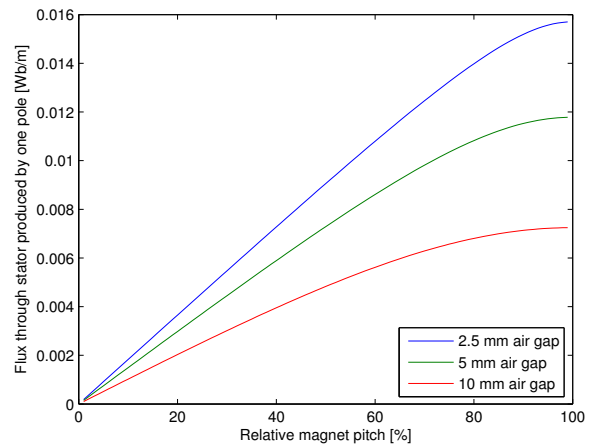

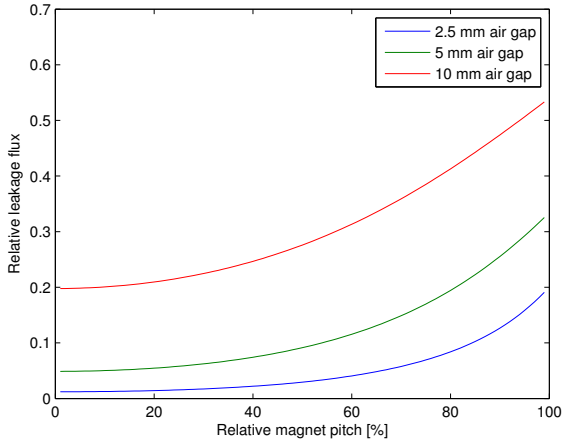Fig. 12.   Flux from one pole crossing the stator disk, per unit length.

Fig. 13.   As the relative magnet pitch increases, so does also the relative leakage flux.

The machine presented in this paper will have a relative magnet pitch of about 50%, and a total air gap of 10 mm. As shown in Figure 16, the maximum flux density in the stator is then about 0.4 T, and the flux distribution is almost triangular shaped. The magnet pitch could therefore have preferably been increased, giving a higher power rating for the machine, and a more sinusoidal stator current.
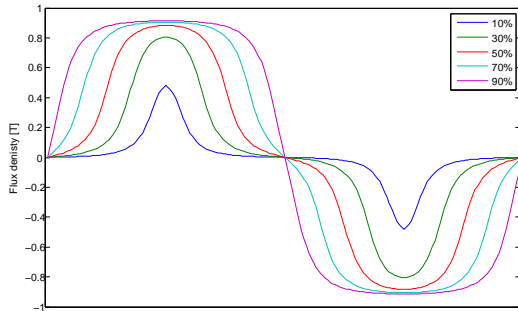

Fig. 14.   Flux distribution over one pole pair for relative magnet pitches of 10%, 30%, 50%, 70% and 90%, 2.5 mm air gap.
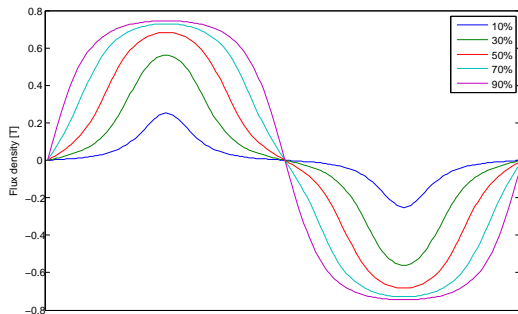

Fig. 15.   Flux distribution over one pole pair for relative magnet pitches of 10%, 30%, 50%, 70% and 90%, 5 mm air gap.
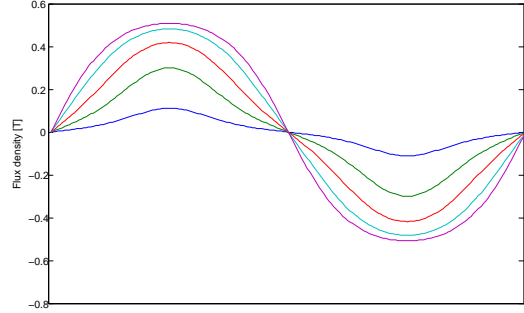

Fig. 16.   Flux distribution over one pole pair for relative magnet pitches of 10%, 30%, 50%, 70% and 90%, 10 mm air gap.

B. Winding factor

Using a method presented in [18], the winding factors are calculated. The winding factor, k_w is the product of the distribution factor, k_d and the pitch factor, k_p:

$$k_w = k_d k_p \qquad (7)$$

The distribution factor is a measure of the loss in induced voltage caused by coils of the same phase not being exactly in phase with each other, as the case is when using fractional or distributed windings. It is defined as the vector sum of the induced voltages in coils belonging to the same phase divided by the the arithmetic sum of these induced voltages, as shown in Figure 17, and is given by (8).
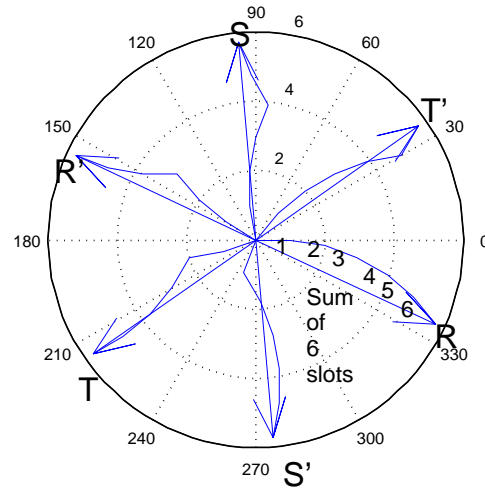
Fig. 17.   Voltage vectors for q=6/5, for both turn and return conductors

$$k_d = \frac{\sin(n\gamma/2)}{n\sin(\gamma/2)} \qquad (8)$$

, where n is the number of different phasors belonging to one phase, and γ is the electrical angle between these. For a 3-phase machine with 60° coil spread, $\gamma = 60^o/n$. For three phase machines with q=12/11 and q=6/5 presented in V-A, the distribution factors are $k_d = 0.9552$ and $k_d = 0.9561$

respectively. For the non-fractional winding with q=1, all the induced voltages belonging to the same phase are totally in phase with each other, so that the distribution factor is 1.

The pitch factor gives a measure of the reduction of induced voltage in one coil caused by a reduction of the coil pitch. The induced voltage of a coil is maximized if the coil spans one pole exactly, as this gives maximum flux linkage for the coil. The pitch factor is calculated using

$$k_p = \cos(\frac{\pi - \rho}{2}) \tag{9}$$

, where ρ is the coil pitch. For q=12/11, the coil pitch is 165°, resulting in a pitch factor of $k_p = 0.9914$, while the coil pitch of 150° for q=6/5 gives a pitch factor of $k_p = 0.9659$. For the non-fractional winding with q=1, the coil pitch of 180° naturally gives a pitch factor of 1.

Multiplying these distribution factors and the pitch factors gives winding factors of $k_w = 0.947$ and $k_w = 0.924$ for q=12/11 and q=6/5 respectively, while the machine with q=1 has a winding factor of 1. By assuming that the copper volume is the same in these stators, and using the same conductor area, it is clear that the number of turns per coil must decreases as the number of coils increases. As the total copper cross section then is unchanged, the total number of turns is also the same for the three machines, so that the winding factors is a measure of the theoretical relative power output of these. However, the coils presented in VI-B, will all have 20 turns, so that the copper amount in the stators varies, with q=6/5 having the most copper and q=1 the least. A machine with q=1 will have 55 coils per phase, q=12/11 has 60, while q=6/5 has 66 coils per phase. Based on this, q=12/11 has an induced voltage being $0.947 \cdot 60/55 = 1.033$ relative to the induced voltage for q=1, while q=6/5 has an induced voltage of $0.924 \cdot 66/55 = 1.109$ relative to q=1. Neglecting any losses, this will also be the relative power of the machines.

C. Maximum allowed losses

The glue used for the stator windings has a maximum operating temperature of 80^oC. In order to have a safety limit, the maximum allowed temperature in the stator is decided to be 70^oC. A thermal model of the stator's cross section is made in COMSOL. As the endturns position vary around the circumference in the machine, they are simplified into a cross section, shown in Figure 18 with an area so that when multiplied with the machines circumference, the volume is the same as the total volume of the windings in the physical machine. It is assumed that the rotation of the rotor provides good ventilation, so that the temperature will be at room temperature, 25^oC, 1 mm away from the copper, regardless of the temperature in the copper. The simulation shows that the heat production may be up to $480000\frac{W}{m^3}$, without exceeding the temperature limit. Multiplying the area used in the COMSOL simulation with a circumference of $\pi \cdot 0.72$ m, the total allowed stator loss is calculated to be 251.2 W.
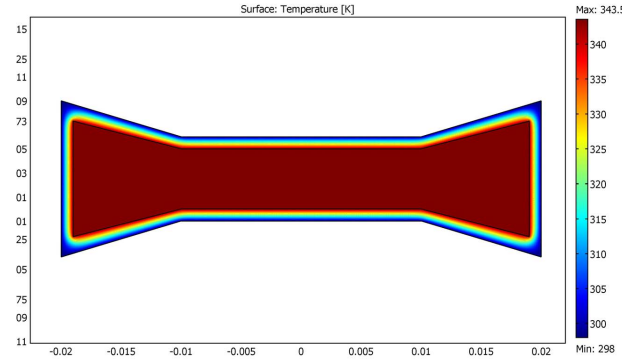

Fig. 18. Thermal model of the stator.

D. Eddy current losses in stator windings

The eddy current losses are calculated using a linearized COMSOL model of the machine, consisting of one pole cut in half at the middle of the air gap with 1 mm stator conductors in three different axial positions. The time varying magnetic field set up by the moving rotor is modeled with a magnet in fixed position, but with a remanent flux density varying sinusoidally from -1.15 T to 1.15. This is done at five different frequencies; 50 Hz, 100 Hz, 200 Hz, 400 Hz and 800 Hz. Because of the high reluctance of the ironless stator, the current in the stator will not produce any significant magnetic field compared to the one produced by the magnets, so that the conductors can be modeled without any current applied. Neither the eddy currents does produce any notable magnetic field, so that the rest of the conductors in the coil and in other phases don't have to be included in the model. The COMSOL model should therefore work for any q. In the real machine, the rotor back iron will not see any notable change in the magnetic field, hence there will be almost no eddy current losses in the rotor back iron. To avoid eddy current losses in the rotor back iron in the COMSOL simulation, the rotor back iron is modeled with zero conductivity. A relative permeability of 4000 is used for the rotor back iron.

Two components of the eddy current losses are considered, the main one is due to the change of axial directed air gap flux, while a smaller component is caused by the change of the tangential directed leakage flux. Losses associated to the air gap flux are modeled by placing the conductors at the center of a magnet pitch, so that the main part of the flux passing through conductors is traveling in the axial direction, as shown in Figure 19. Losses associated by the tangential leakage flux is modeled by placing the conductors just between two poles, so that the main part of the flux passing through the conductors is traveling in the tangential direction, as shown in Figure 20.

It should be commented that the model for eddy current losses caused by the tangential leakage flux has some unsolved errors. For unknown reasons, the COMSOL model gives unreasonable high values when modeling the half-conductors indicated in the left of Figure 20 as copper, they are in this
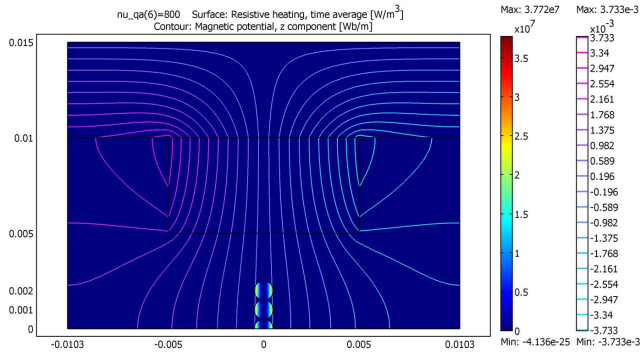
Fig. 19.   COMSOL model for calculating eddy current losses caused by air gap flux.

Fig. 20.   COMSOL model for calculating eddy current losses caused by leakage flux.

model therefore modeled as air. As mentioned above, the flux produced by the eddy currents will not have any notable impact on the magnetic field in the machine, so that the left half-conductors can be omitted in the simulation. The right conductors, in which the eddy current losses are calculated, are modelled as copper. Another inintelligible behavoir of the model is that the lower conductor being positioned at the middle of the airgap, where the tangential leakage flux is approximately zero, experiences losses bigger than the conductor above it. The cause of this may be that the air gap flux is not totally excluded in this model, with a maximal air flux of about 0.02 T against a maximal tangential leakage flux of about 0.1 T in the area where the conductors are

placed, so that some of the losses in the tangential leakage flux component is caused by air gap flux. This will especially be the case for the conductor placed in the middle of the air gap. Therefore, the losses in this particular conductor is not taken into account when calculating the total eddy current losses caused by the tangential leakage flux.
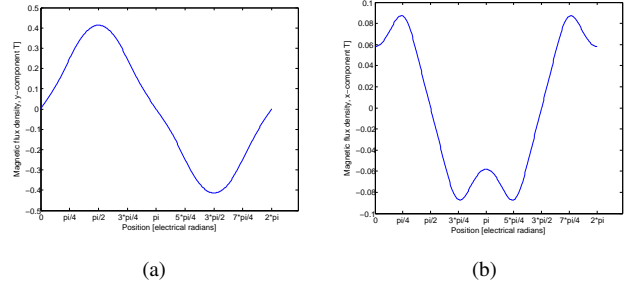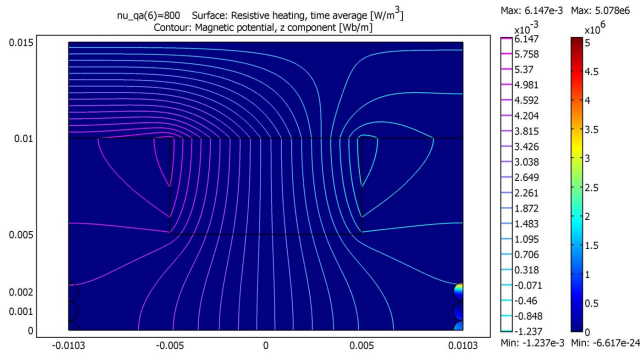

Fig. 21.   y-component of the flux density at the middle of the airgap (a) and x-component of the flux density at the middle of the airgap (b).

It is here assumed that these two flux components will vary sinusoidally as the coil is moving through the magnetic field, while Figure 21 shows that this is not the case. The air gap flux is somewhat triangular shaped, but as the frequency and amplitude is correct, this deviation should not have a significant impact on the eddy current losses. The tangential leakage flux differs more, with a different maximum value than the value existing just between the poles, and a large third harmonic component. Therefore, the value of the eddy current losses caused by the tangential leakage flux is probably larger than what is calculated here. The eddy current losses for frequencies of 50 Hz, 100 Hz, 200 Hz, 400 Hz and 800 Hz are presented in Table VII-D.

TABLE II
SIMULATED EDDY CURRENT LOSSES

Frequency [Hz]	Air gap flux losses [W]	Leakage flux losses [W]	Total losses [W]
50	4.2	3.8	8
100	16.8	4.9	21.7
200	67.1	9.1	76.3
400	268.5	26.0	294.5
800	1073.5	48.0	1121.5

E. Maximum allowed phase current

The machine uses circular conductors with a diameter of 1 mm. The total length of each phase, including coils and 50 mm connections between the coils are calculated to be 122.8 m for q=1, 129.8 m for q=12/11 and 138.3 m for q=6/5. Using a resistivity of $2.08 \cdot 10^{-8} \Omega m$ at 70^oC for the copper, the phase resistance is 3.13 Ω for q=1, 3.31 Ω for q=12/11 and 3.53 Ω for q=6/5. Based on VII-C, the maximum total heat production in the windings should be less than 251 W in order to keep the stator temperature below 70^oC. Subtracting 8 W of eddy current losses at 50 Hz, the total allowed resistive losses are 243 W, giving maximum rms phase currents of 5.09 A for q=1, 4.95 A for q=12/11 and 4.79 A for q=6/5.

F. Inductance

1) Analytic inductance calculation: The self inductance of a phase is calculated using a method presented in [5]. The inductance of the machine can be split into two parts; the armature reaction inductances, L_a, and the leakage inductance, $L_{l}eak$.

$$L_d = L_a + L_{leak} \tag{10}$$

For a machine with surface mounted magnets and a relative permeability in the magnets close to 1, the equivalent airgap-length is nearly the same in both d- and q-axis, so that it's not necessary to separate between these inductances[5].

L_a is calculated by

$$L_a = \frac{m\mu_0}{\pi}\left(\frac{2Nk_w}{p}\right)^2\frac{R_{out}^2 - R_{in}^2}{g_{eq}} \tag{11}$$

, where $\mu_0 = 4\pi \cdot 10^{-7}$ N/A^2 is the vacuum permeabilty, $m = 3$ is number of phases, $N = 20 \cdot 66 = 1320$ is the total number of turns per phase, $k_w = 0.924$ is the winding factor from VII-B, $p = 110$ is the number of poles, and $R_{out} = 0.37$ m and $R_{in} = 0.35$m is the outer and inner radius of the airgap. $g_{eq} = 22.66$ mm is the equivalent airgap distance, given by

$$g_{eq} = 2[g + 0.5t_w + \frac{h_M}{\mu_r}] \tag{12}$$

, in which $g = 4$ mm is the one sided axial distance between the coils and the magnet surface, $t_w = 5$ mm is the axial thickness of the active part of the coils, $h_M = 5$ mm is the axial thickness of one magnet, and $\mu_r = 1.035$ mm is the relative permeability of the magnets.

The leakage inductance consists of three parts, the leakage inductance due to the radial portions of the conductors, L_s, the leakage inductance due to the endturns, L_e, and the differential leakage inductance due to higher space harmonics, L_d, with specific permeances of λ_s, λ_e and λ_d respectively.

$$L_{leak} = L_s + L_e + L_d \tag{13}$$

, with

$$L_s = 4\mu_0\frac{N^2(R_{out} - R_{in})}{pq}\lambda_s \tag{14}$$

$$L_e = 4\mu_0\frac{N^2(R_{out} - R_{in})}{pq}\frac{l_e}{R_{out} - R_{in}} \tag{15}$$

$$L_d = 4\mu_0\frac{N^2(R_{out} - R_{in})}{pq}\lambda_d \tag{16}$$

, where $q = 6/5$ is the number of coil sides per pole per phase, $l_e = 17.14$ mm is the length of an endturn, and $\lambda_s \approx 0.36$ and $\lambda_e \approx 0.36$ is given by the semi-analytical equation:

$$\lambda_s \approx \lambda_e \approx 0.3q \tag{17}$$

λ_d is rather small at 50 Hz , and is difficult to calculate precisely. As λ_d is assumed to have a minor influence relative

on the total leakage inductance compared to the uncertainties in the other two permeances, it is neglected.

Using these equations with the proper vaules, $L_a = 0.3746$ mH, $L_s = 0.4777$ mH and $L_e = 0.4093$ mH, so that the total phase inductance of the machine is $L_d = 1.262$ mH.

2) Inductance calculation by FEM: The inductance corresponding to the flux caused by the radial portions of the conductors is also calculated using a COMSOL simulation on a tangential cross section of the linearized machine, as shown in Figure 22. The coils of one phase, even though in series, will not affect each other in terms of inductance, and the superposition principle is therefore valid. Even though it therefore is sufficient to model one coil alone, the entire rotor back iron rings must be modeled, as this affects the reluctance for the MMF set up by the coil. The rotor magnets does not affect the inductance, and they are therefore not drawn. However, the magnets have a relative permeability of 1.035, affecting the average reluctance seen from the stator coils. This is represented by a 5 mm layer with a permeability of $\mu_{r,avg} = 1.035\tau_m/\tau_p + (\tau_p - \tau_m)/\tau_p = 1.017$, while the rotor back iron is given a relative permeability of 5000. Each coil side's cross section is modeled as one square shaped conductor with area $A = 4 \cdot 5$ mm^2. The coil in center of the model is given a current density of $J = 1$A/mm^2, equivalent to a current of $I = 1$ A in each of the 20 conductors constituting a coil in the real machine.
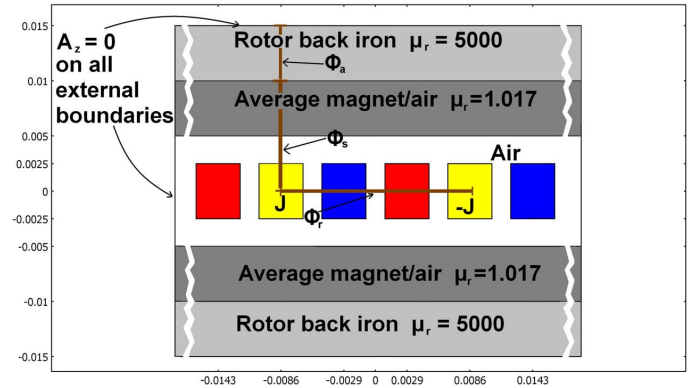
Fig. 22. Model for inductance calculation.

By integrating the flux density over the three lines shown in Figure 22, and multiplying by the radial length of 20 mm, the flux values are found to be $\phi_r = 0.5399$ μWb, $\phi_a = 0.1585$ μWb and $\phi_s = 0.1114$ μWb. The inductance L is given by (18).

$$L = \frac{\lambda}{I} = \frac{N_t\phi_r}{I} \tag{18}$$

, where λ is the flux linkage, and N_c is the number of conductors in the coil [19]. The inductance corresponding to the flux produced by the radial part of the coil, is by equation (18) calculated to be $L_r = 10.798$ μH. As seen in Figure 23, the flux produced by one coil splits into two symmetrical parts that further consist a flux portion that crosses the airgap, ϕ_a, and a flux portion that does not, ϕ_s, so that $\phi_r = 2(\phi_a + \phi_s)$.
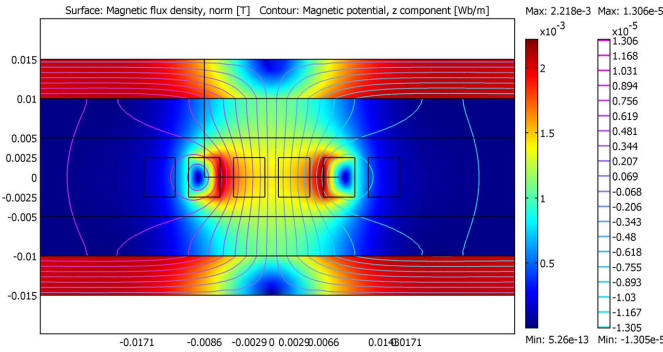
Fig. 23.   Magnetic field produced by one coil.
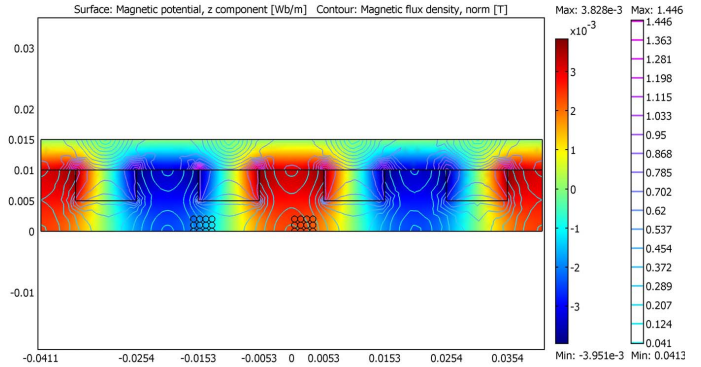
Fig. 24.   COMSOL solution for the magnetic potential in the machine.

Corresponding to this, the total inductance due to the radial part of the coil may be split into an armature component and a radial leakage component; $L_r = L_a + L_s$. Using (18), $L_a = 6.34$ μH and $L_s = 4.46$ μH. For the 66 coils of one phase of the machine, the inductance due to radial parts of the coils is $L_r = 0.713$ mH, of which $L_a = 0.418$ mH and $L_s = 0.294$ mH. L_a is here somewhat larger than the analytical value, while L_s is significantly smaller.

G. Induced voltage

A linearized COMSOL model used for calculating the induced voltage is presented in Figure 24. Due to the symmetry in the middle of the airgap, it's sufficient to model only half of the machine. The rotor back iron is modeled with a relative permittivity of 4000, while the magnets have a remanent flux density of ± 1.15 T in the y-direction. The upper boundary is given magnetic insulation, while all the other outer boundaries are modeled with electrical insulation. As the conductors are made of copper, they do not have any impact on the field solution. For all the conductors, the magnetic potential is found as a function of the position in the x-direction. By differentiating the flux passing through each turn with respect to time, and adding these together, the induced voltage for a coil is found as a function of time. Subsequently, the induced voltages for all the coils within one phase are added together giving the total induced voltage in the machine. For q=12/11 and q=6/5, the phase difference of the coils within one phase must be taken into account.

The induced three phase voltage and the neutral voltage of machines with q=1, q=12/11 and q=6/5 running at 50 Hz is presented in Figure 25. The voltage waveforms are quite triangular shaped, due to the small relative magnet pitch, as mentioned in VII-A. Using the fft-function in MATLAB, the harmonic spectrum of a induced single phase voltage is obtained. As shown in Table III, the third harmonics are significant, and the THD rather large. Changing the q has some impact on the THD, but not very much. One should note that q=6/5 has the highest induced voltage, while q=1 has the lowest. This is because the machine not being optimized in terms of copper in the stator; as discussed in VII-B, the number of turns per coil are kept constant in the three stators, while the amount of copper is changing.
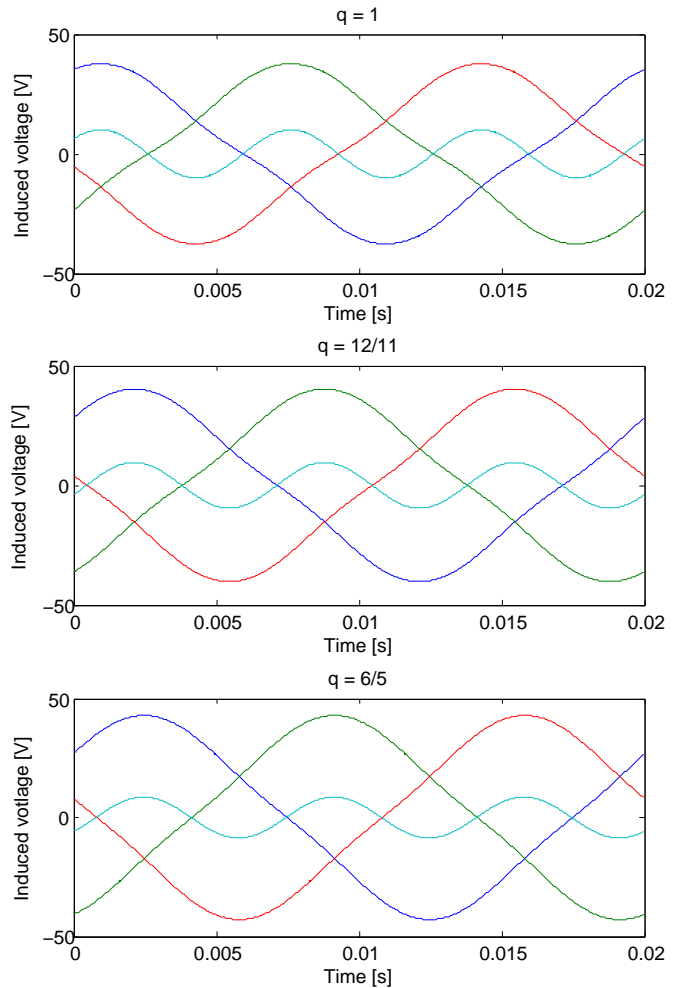

Fig. 25.   3 phase induced voltage and neutral voltage for machines with q=1 (top), q=12/11 (middle) and q=6/5 (bottom).

q	1st [V]	3rd [%]	5th [%]	7th [%]	THD [%]
1	34.73	9.59	1.11	0.18	9.66
12/11	37.34	8.56	0.74	0.10	8.60
6/5	40.22	7.18	0.39	0.04	7.19

H. Power output

As the reactance of the machine is quite low, it is assumed that the machine operates close to unity power factor. All three winding configurations apply conductors with diameters of 1 mm, but the maximum allowed current differs from 5.09 A$_{RMS}$ for q=1, 4.95 A$_{RMS}$ for q=12/11 and 4.79 A$_{RMS}$ for q=6/5, as of described in VII-E. Assuming a pure resistive load, the current waveform will be of the same shape as the voltage. The amplitude values of these somewhat triangular shaped currents corresponding to the maximum allowed RMS currents are 7.77 A for q=1, 7.51 A for q=12/11 and 7.21 A for q=6/5. Multiplying the currents and phase voltages together results in the power production of 377 W for q=1, 393 W for q=12/11 and 410 W for q=6/5 at 50 Hz, of which 251.2 W will be lost as heat in the stator, see VII-C. The maximum power output is then 125.8 W for q=1, 141.8 W for q=12/11 and 158.8 W for q=6/5, with efficiencies of 33%, 36% and 39% respectively. These low values are mostly due to the long endturns, causing the resistance to be very high compared to the induced voltage. As seen in Table VII-D, the frequency can be increased while still maintaining the eddy current losses at a reasonable level, resulting in a higher induced voltage. The machine will therefore perform better in terms of electrical efficiency if run at higher speeds.

The fluctuations of the power produced are presented in Figure 26, being 1.8% for the q=1, 1.1% for q=12/11 and 0.5% for q=6/5. One should note that in the design presented in this thesis, the number of turns per coil are kept constant for the three machines, so that the more coils in the machine, the more copper in total. In an optimized machine on the other hand, the total amount of copper would probably be kept constant, while the number of turns per coil would decrease as the number of coils increase. In that case, the induced voltage of the machine would decrease as the fraction q increases, as discussed in VII-B.

VIII. MEASUREMENTS

At the moment, only one segment of a stator with q=6/5 is made. All measurements are done on this segment, covering 2/11 of the machine. The machine is only tested in generator mode, with a pure resistive load. Because of lack of time, a rather unsuited prime mover was used; a 50 W DC motor with a rated speed of 4000 rpm. Even though there was a reduction gear between the DC motor and the generator, the DC motor had to operate far below this rated speed, and was not able to deliver sufficient torque to the machine so that it could be run steady state with any load. The load tests are therefore done by accelerating the machine up to a high speed before applying any load, so that the measurements are done while the machine
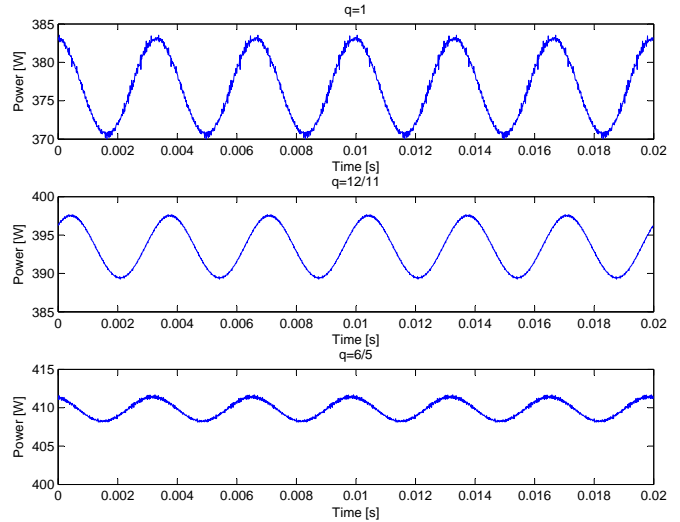
Fig. 26. Power fluctuations for machines with q=1 (top, q=12/11 (middle) and q=6/5 (bottom).

is de-accelerating. Because of this, it was not possible control or read the frequency during the tests, so that the frequencies presented are found by manually examining the waveforms of the oscilloscope. There are not done any full load tests of the machine, and even though the stator had temperature sensors implemented, it was not loaded for a sufficient time to notice any temperature response.

A. Resistance

The DC phase resistance is measured with a RLC meter, with results presented in table IV.

DC resistance [Ω]		
R	S	T
0.457	0.458	0.454

The DC resistance at 70°C of a complete stator is in VII-E calculated to be 3.53 Ω. This corresponds to a resistance of 0.525 Ω at 20°C for a stator segment, somewhat higher than the measured values.

B. Inductance

The stator segment phase self inductances are measured with an RLC meter, with results presented in Table V. By applying AC current measured with a multimeter in one phase, and measuring the induced voltages in the two others with oscilloscope, the mutual inductances are found. In order to reduce the inaccuracies involved, several measurements, were done. The inaccuracy for the obtained values are 2 %, indicating that the mutual inductances presented in Table V are different beyond the uncertainty in the measurements. A reason for this may be that the coils at the ends of the

TABLE V
INDUCTANCE FOR A STATOR SEGMENT WITH Q=6/5, COVERING 2/11 OF
THE MACHINE

	Inductance [μH]		
	R	S	T
R	102	49	47
S	49	104	50
T	47	50	106

segmented stator are not linked to coils on both sides, which they would be if the stator was complete.

In VII-F, the self inductance of a phase for the entire stator is analytically found to be $L_d = 1.262$ mH, which correspond to 229 μH for a stator segment. This value is for unknown reason more than twice the value found by measurements. The COMSOL simulations for the active parts only of the conductors equals an inductance of 130 μH for a stator segment, still larger than the measure value.

C. Induced voltage

The induced voltage in each of the three phases, being isolated from each other, are measured using a oscilloscope. The result at 74 Hz is presented in Figure 27. One can see that induced voltage is rather triangular shaped, and by using the fft-function in MATLAB, it is found that the third harmonic constitutes 2.7% of the induced voltage, significantly lower than the simulated value presented in Table III.
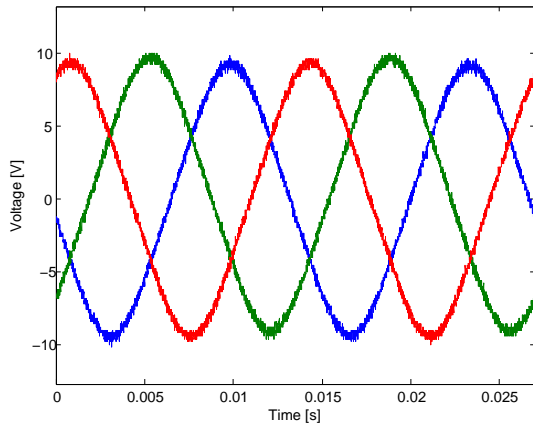
Fig. 27. Induced voltage in a stator segment. The phases are in this measurement are isolated from each other.

The line to line voltages at open circuit are measured at 92 Hz with the generator having an isolated neutral point. As shown in Figure 28, the line voltage is rather sinusoidal shaped, with third the harmonics amplitude constituting 0.4% of the total amplitude.

The generator was tested at several frequencies, with the amplitudes of the induced voltages are presented in Table VI. The fraction V/f is more or less constant for all tests, indicating a linear relationship between the speed and the induced voltage when the inaccuracies in the readings are taken into account.

The amplitude of the fundamental of phase voltage is in VII-G simulated to be 40.22 V at 50 Hz for a complete stator,
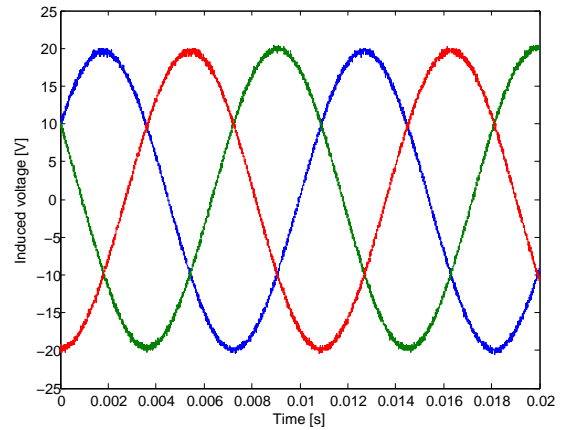
Fig. 28. Induced voltage in a stator segment at 92 Hz. The phases share an isolated neutral point.

TABLE VI
INDUCED LINE-LINE VOLTAGE AT NO-LOAD.

f [Hz]	$V_{ll,ampl}$ [V]	$V_{ll,ampl}/f$ [V/Hz]
37	8.7	0.24
55	12.5	0.23
92	20.2	0.22
133	29.3	0.22
172	37.8	0.22

meaning that the line-line voltage of a stator segment will be $40.22\text{V} \cdot \sqrt{3}\,11/2 = 12.7$V. The simulated fraction V/f is thereby 0.25, which is rather close to measured the values presented in Table VI.

D. Power output

The generator is connected is tested with two different resistive loads, at various speeds. The two loads consist of three resistors of either 80 Ω or 40 Ω, connected in a delta configuration. Figure 29 presents the phase-neutral voltage and the phase current at 155 Hz when the generator is connected to a delta connected load with 80 Ω. The third harmonics constitutes 4.6% of the amplitude of the phase-neutral voltage, while they are not detectable in the current.

Assuming that the phases are symmetrical, the total power output calculated based on these two values, and is presented in Figure 30

From Table VI on can see that the ratio between the amplitude of the induced line-line voltage and frequency is about 0.23, or 0.13 between the amplitude of the induced phase-neutral voltage and the frequency. Table VII presents the induced phase neutral voltage, E, calculated using this assumed-to-be-constant relationship, in addition to the measured phase-neutral voltage, V_{pn}, and the phase current, I. Based on this information, it should be possible to find the voltage drop within the generator, and thereby the impedance of the machine. Unfortunately, the measurements are too inaccurate for this: This is the case for both the ratio between speed and induced voltage, and the frequency, which is found manually by examining the plots from the oscilloscope. Therefore, the theoretical induced voltages for each of the tests in Table

Fig. 29.   Phase-neutral voltage and phase current at 155 Hz with a delta connected 80 Ω load.

Fig. 30.   Power output at 155 Hz with a delta connected 80 Ω load.

VII is highly unreliable, exemplified by the fact that some of the measured voltages are higher than their corresponding theoretical induced voltages.

TABLE VII
PERFORMANCE AT DIFFERENT LOADS LEVELS

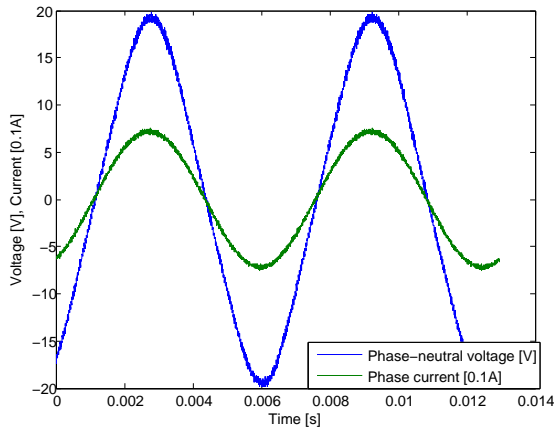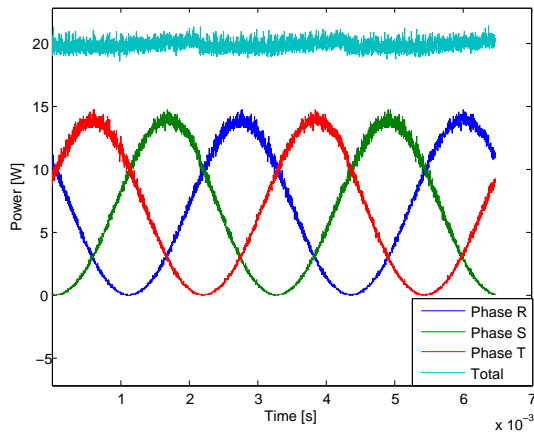| f [Hz]	$E_{pn,ampl}$ [V]	$V_{pn,ampl}$ [V]	$I_{p,ampl}$ [A]	3-phase power output [W]
125	16.25	15.0	1.06	23.9
97	12.61	12.6	0.87	16.4
65	8.45	8.4	0.59	7.4
29	3.77	3.7	0.26	1.4
155	20.15	19.8	0.75	22.3
155	20.15	19.9	0.75	22.4
116	15.08	15.2	0.57	8.7
81	10.53	10.6	0.40	6.4
48	6.24	6.3	0.24	2.7

IX. FUTURE WORK

At the moment, only a stator segment covering 2/11 of a complete stator with q=6/5 is made. Even though this segment provides electrical symmetry, so that the machine can be run on this alone, it is planned to make more segments to make the stator complete. As described in VI-E, some small changes should be done when producing the stator, in order to give better clearing between the stator and the rotors. This should not affect the electrical behavior of the machine. The stator segments should be made with adjustment bolts for more controlled positioning in the airgap. The rotor rings should be either flattened, or positioned more accurate.

Other windings types should be made and tested out in the machine. Firstly, the similar 3-level-endturn windings with q=1 and q=12/11 presented in this text should be constructed, so a comparison between these and the existing design can be done. Also 2-level-endturn windings and non-overlapping windings may be tested in the rig. In order to make proper tests, a more suited prime mover should be implemented.

For use as a demonstration model, it should be possible to mount a handle to the shaft, so the machine can be run be hand. This will give the user an experience of how the electrical frequency and the amplitude of the induced voltage varies with the speed of the machine. It may also be an idea to mount a load consisting of light bulbs or an small induction motor on the rig, so that the power produced is visualized. As all the active parts of the generator is possible, this would give a good illustration of the conversion between mechanical to electrical energy.

X. CONCLUSION

An ironless stator axial flux 110 pole dual rotor permanent magnet machine is made. The purpose of the machine is to be a test setup for different ironless stator winding topologies. A stator frame for easily inserting different types of stator segments at the same time is implemented. The machine is made in such a way that all active parts are visible, and is therefore well suited as a demonstration model for electrical rotating machines. Three different single layer overlapping 3-level-endturn windings, with q=1, q=6/5 and q=12/11, have been simulated and designed. At the moment only one stator segment with q=6/5, covering 2/11 of the stator is constructed. The machine presented is not at all optimal in terms of efficiency or cost, but decisions on the design has rather been made on basis of available parts and ease of construction. Anyhow, the machine setup designed is well suited for experimental purposes.

Because of a magnet-pitch/pole-pitch ratio of nearly 0.5, the magnetic field at the air gap of the machine is rather triangular shaped. The machine has inner and outer active diameters of 0.70 m and 0.74 m, while the pole pitch is 20.56 mm, which results in endturns constituting a large part of the winding. The DC resistance is therefore rather large, 0.46 Ω, compared to to the induced line-line voltage amplitude of 12.5 V at 55 Hz for the segment. This values are quite close to the simulated ones. The self and mutual inductance of a stator segment are measured being 100 μH and 50 μH, with the self inductance being less than half of the calculated values. The machine is connected to a resistive load, and the output have been studied. However, because of lack of both time and a suitable prime mover, the machine has not been run at full load, and no detailed tests have been done with the machine supplying a load.

REFERENCES

[1] Ghalamestani and Husum, *Ocean Wave Energy Converter*, M.Sc specialization project, NTNU, 2007.

[2] Nilssen, *Forslag til bolgekraftverk med en flytende enhet og et fullstendig lukket system*, NTNU, unpublished.

[3] *Homopolar generator*, http://en.wikipedia.org/wiki/Homopolar_generator, [Internet, last accessed 27 June 2008]

[4] Davenport, *Improvement in propelling machinery by magnetism and electromagnetism.*, U.S. Patent No. 132

[5] Gieras, Wang and Kamper, *Axial Flux Permanent Magnet Brushless Machines*, Kluwer academic publishers, Dordrecht/Boston/London, 2004

[6] Patterson, Brice, Dougal and Kovuri, *The "Goodness" of Small Contemporary Permanent Magnet Electric Machines*, IEEE International Electric Machines and Drives Conference, 2003. vol. 2, pp 1195 - 1200, June 2003

[7] Caricchi, Crescimbini, Fedeli and Noia, *Design and Construction of a Wheel-Directly-Coupled Axial-Flux PM Motor Prototype for EVs*, Conference Record of the 1994 IEEE Industry Applications Society Annual Meeting, vol. 1, pp 254-261, Oct 1994

[8] Chen, Pillay and Khan, *PM Wind Generator Comparison of Different Topologies*, Conference Record of the 2004 IEEE 39th Industry Applications Conference, 2004, vol. 3, pp 1405 - 1412, Oct 2004

[9] Spooner, Gordon, Bumby and French, *Lightweight ironless-stator PM generators for direct-drive wind turbines*, Electric Power Applications, IEE Proceedings, vol. 152, Issue 1, pp 17-26, Jan 2005

[10] Greaves, Walker and Walsh, *Design optimisation of Ironless Motors based on Magnet selection*, Journal of Electrical & Electronics Engineering, Australia, IEAust, vol. 21, no. 1, pp. 49-56, 2001.

[11] Wang and Kamper, *Evaluation of Eddy Current Losses in Axial Flux Permanent Magnet (AFPM) Machine with an Ironless Stator*, Conference Record of the 37th Industry Applications Conference Annual Meeting. vol 2, pp 1289 - 1294, October 2002

[12] Caricchi, Crescimbini, Honorati, Lo Bianco and Santini, *Performance of Coreless-Winding Axial-Flux Permanent-Magnet Generator with Power Output at 400 Hz, 3000 r/min*, IEEE Transactions on industry applications, vol. 34, no. 6, pp 1263-1269, December 1998.

[13] Del Ferraro, Terrigi and Guilii Capponi, *Coil and Magnet Shape Optimization of an Ironless AFPM Machine by Means of 3D FEA*, IEEE International Electric Machines & Drives Conference '07. , vol. 2, pp 927-931, May 2007.

[14] Hill-Cottingham, Coles, Eastham, Profumo, Tenconi and Gianolio, *Multi-disc axial flux Stratospheric Aircraft Propeller Drive*, Conference Record of the Thirty-Sixth IEE Industry Applications Conference Annual Meeting. vol. 3, pp 1634-1639, October 2001.

[15] Kamper, Wang and Rossouw, *Analysis and Performance Evaluation of Axial Flux Air-Cored Stator Permanent Magnet Machine with Concentrated Coils*, IEEE International Electric Machines & Drives Conference '07. , vol. 1, pp 13-20, May 2007.

[16] Wang, Kamper, Van der Westhuizen and Gieras, *Optimal Design of a Coreless Stator Axial Flux Permanent Magnet Generator*, IEEE Transactions on magnetics, vol. 41, no. 1, pp 55-64, January 2005.

[17] Noddeland, *Repulsive Passive Magnetic Bearing for Large Diameter Applications*, M.Sc specialization project, NTNU, 2006.

[18] Fitzgerald, Kingsley and Umans, *Electric Machinery*, 5th edition, McGraw-Hill, New York, 1990.

[19] Young and Freedman, *University Physics with modern physics*, 11th edition, Pearson/Addison Wesley, San Francisco, 2004

```matlab
% COMSOL Multiphysics Mdel M-file
% Generated by COMSOL 3.3 (COMSOL 3.3.0.405, $Date: 2006/08/31 18:03:47 $)

flclear fem
clear all
clc


% COMSOL version
clear vrsn
vrsn.name = 'COMSOL 3.3';
vrsn.ext = '';
vrsn.major = 0;
vrsn.build = 405;
vrsn.rcs = '$Name:  $';
vrsn.date = '$Date: 2006/08/31 18:03:47 $';
fem.version = vrsn;

gapindex = 0;
for air_gap = [0.0025, 0.005, 0.01];
gapindex = gapindex+1;

magnet_thickness = 0.005;
rbi_thickness = 0.005;
pole_pitch = 0.02;
k = 0;                          %Counter
for rel_mag_pitch = 0.1:0.2:0.9
   k = k+1;                     %Counter
   mag_pitch = rel_mag_pitch*pole_pitch;

% Geometry
g1=rect2(pole_pitch,air_gap/2+magnet_thickness+rbi_thickness,'base','corner','pos',[-0.01,0]);
g2=rect2(pole_pitch,rbi_thickness,'base','corner','pos',[-0.01,air_gap/2+magnet_thickness]);
g3=rect2(mag_pitch,magnet_thickness,'base','center','pos',[0,air_gap/2+magnet_thickness/2]);

% Analyzed geometry
clear s
s.objs={g1,g2,g3};
s.name={'R1','R2','R3'};
s.tags={'g1','g2','g3'};

fem.draw=struct('s',s);
fem.geom=geomcsg(fem);

% Initialize mesh
fem.mesh=meshinit(fem, ...
         'hauto',5);



% Refine mesh
fem.mesh=meshrefine(fem, ...
          'mcase',0, ...
          'rmethod','regular');

% Application mode 1
clear appl
appl.mode.class = 'FlPerpendicularCurrents';
appl.assignsuffix = '_qa';
clear bnd
bnd.type = {'tH0','cont','A0'};
bnd.ind = [1,1,1,2,3,2,2,2,2,2,1,1];
appl.bnd = bnd;
clear equ
equ.magconstrel = {'mur','Br','mur'};
equ.Br = {{0;0},{0;1.15},{0;0}};
equ.mur = {1,1,5000};
equ.ind = [1,3,2];
appl.equ = equ;
fem.appl{1} = appl;
fem.frame = {'ref'};
fem.border = 1;
clear units;
```

```matlab
units.basesystem = 'SI';
fem.units = units;

% Multiphysics
fem=multiphysics(fem);

% Extend mesh
fem.xmesh=meshextend(fem);

% Solve problem
fem.sol=femstatic(fem, ...
            'solcomp',{'Az'}, ...
            'outcomp',{'Az'});

% Save current fem structure for restart purposes
fem0=fem;

% Integrate
stat_flux(k,gapindex)=postint(fem,'By_qa', ...
        'unit','Wb', ...
        'dl',[2], ...
        'edim',1);

% Integrate
leak(k,gapindex)=postint(fem,'Bx_qa', ...
        'unit','Wb/m', ...
        'dl',[1], ...
        'edim',1);

% Integrate
aak(k,gapindex)=postint(fem,'Bx_qa', ...
        'unit','Wb/m', ...
        'dl',[3], ...
        'edim',1);

s=0:0.01:1;
flux_gap(1:length(s),k,gapindex) = postinterp(fem, 'By_qa', s, 'dom',2);

flux_gap(length(s)+1:2*length(s)-2,k,gapindex) = -flux_gap(2:length(s)-1,k,gapindex);

plot(flux_gap)

end
end
```

APPENDIX 2: Resistance calculation

Resistance calculation

Maximum allowed tempereture in machine	70	[C]
Room temperature	25	[C]
Qtot per volume, max from COMSOL	480000	[W/m^3]
Copper volume in COMSOL	0.00052341	[m^3]
Qtot, max in COMSOL	251.238945	[W]
Q Eddytot at 50 Hz	8	[W]
Q resistive at 50 Hz, 70 degrees	243.238945	
Qphase, max, in COMSOL	81.0796483	[W]

Copper specific resistance at 20 degrees	1.68E-08	[ohm*m]
Copper specific resistance at 70 degrees	2.01E-08	[ohm*m]
Conductor diameter	1	[mm]
Conductor area	0.78539816	[mm^2]
Conductor resistance per meter	2.55E-02	[ohm/m]

Mean coil length	34	[mm]
Turns per conductor	20	
Assumed length between coils	50	[mm]

q=1:

Mean coil width	20.56	[mm]
Conductor length in coil, incl connection	2232.4	[mm]
Number of coils per phase	55	
Length of conductor in phase	122782	[mm]
Phase resistance	3.13E+00	[ohm]
Iphase, max, rms	5.09	[A]

q=12/11:

Mean coil width	18.85	[mm]
Conductor length in coil, incl connection	2164	[mm]
Number of coils per phase	60	
Length of conductor in phase	129840	[mm]
Phase resistance	3.31E+00	[ohm]
Iphase, max, rms	4.95	[A]

q=6/5:

Mean coil width	17.14	[mm]
Conductor length in coil, incl connection	2095.6	[mm]
Number of coils per phase	66	
Length of conductor in phase	138309.6	[mm]
Phase resistance	3.53E+00	[ohm]
Iphase, max, rms	4.79	[A]

```matlab
% COMSOL Multiphysics Model M-file
% Generated by COMSOL 3.3 (COMSOL 3.3.0.405, $Date: 2006/08/31 18:03:47 $)

flclear fem
clear all
clc

format ('long')

% COMSOL version
clear vrsn
vrsn.name = 'COMSOL 3.3';
vrsn.ext = '';
vrsn.major = 0;
vrsn.build = 405;
vrsn.rcs = '$Name:  $';
vrsn.date = '$Date: 2006/08/31 18:03:47 $';
fem.version = vrsn;

tellerting = 0;

for q =6/5%[1, 12/11, 6/5]

tellerting=tellerting+1;

tau_p = 0.720*pi/110;                          %[m]   Pole pitch
tau_c = tau_p/q;                               %[m]   Coil pitch
tau_m = 0.01;                                  %[m]   magnet pitch
el_freq = 50;                                  %[Hz]  Electrical frequency


i=0;                                %Counter

res_lev = 1;                                   %[1]   Must be integer. Determines the step size.
stepsize = tau_p/(72*res_lev);

for pos = [-tau_p/2 : stepsize : tau_p/2]

   i = i + 1

% Geometry
g1=rect2(0.015,4*tau_p,'base','corner','pos',[0,-2*tau_p]);          %Simulation area
g2=rect2(0.0050,4*tau_p,'base','corner','pos',[0.01,-2*tau_p]);      %Rotor back iron

%Magnets
g3=rect2(0.0050,tau_m,'base','corner','pos',[0.0050,tau_p+(tau_p-tau_m)/2]);        %Magnet
g4=rect2(0.0050,tau_m,'base','corner','pos',[0.0050,(tau_p-tau_m)/2]);              %Magnet
g5=rect2(0.0050,tau_m,'base','corner','pos',[0.0050,-(tau_p+tau_m)/2]);             %Magnet
g6=rect2(0.0050,tau_m,'base','corner','pos',[0.0050,-tau_p-(tau_p+tau_m)/2]);       %Magnet

%Conductors
g15=circ2(5.0E-4,'base','center','pos',[0,-5.0E-4+pos]);
g16=circ2(5.0E-4,'base','center','pos',[0.0010,-5.0E-4+pos]);
g17=circ2(5.0E-4,'base','center','pos',[0.0020,-5.0E-4+pos]);
g18=circ2(5.0E-4,'base','center','pos',[0,-0.0015+pos]);
g19=circ2(5.0E-4,'base','center','pos',[0.0010,-0.0015+pos]);
g20=circ2(5.0E-4,'base','center','pos',[0.0020,-0.0015+pos]);
g21=circ2(5.0E-4,'base','center','pos',[0,-0.0025+pos]);
g22=circ2(5.0E-4,'base','center','pos',[0.0010,-0.0025+pos]);
g23=circ2(5.0E-4,'base','center','pos',[0.0020,-0.0025+pos]);
g24=circ2(5.0E-4,'base','center','pos',[0,-0.0035+pos]);
g25=circ2(5.0E-4,'base','center','pos',[0.0010,-0.0035+pos]);
g26=circ2(5.0E-4,'base','center','pos',[0.0020,-0.0035+pos]);

%Cuts conductors in two along the line of symmetry
g28=rect2(0.0010,0.0010,'base','center','pos',[-5.0E-4,-5.0E-4+pos]);
g29=rect2(0.0010,0.0010,'base','center','pos',[-5.0E-4,-0.0015+pos]);
g30=rect2(0.0010,0.0010,'base','center','pos',[-5.0E-4,-0.0025+pos]);
g31=rect2(0.0010,0.0010,'base','center','pos',[-5.0E-4,-0.0035+pos]);
g33=geomcomp({g24,g31},'ns',{'C10','R10'},'sf','C10-R10','edge','none');
g34=geomcomp({g21,g30},'ns',{'C7','R9'},'sf','C7-R9','edge','none');
g35=geomcomp({g18,g29},'ns',{'C4','R8'},'sf','C4-R8','edge','none');
```

```
g36=geomcomp({g15,g28},'ns',{'C1','R7'},'sf','C1-R7','edge','none');
g37=geomcomp({g36},'ns',{'CO4'},'sf','CO4','edge','none');

%Points in the middle of each conductor
parr={point2(0,-5.0E-4+pos)};
g38=geomcoerce('point',parr);
parr={point2(0.0010,-5.0E-4+pos)};
g39=geomcoerce('point',parr);
parr={point2(0.0020,-5.0E-4+pos)};
g40=geomcoerce('point',parr);
parr={point2(0,-0.0015+pos)};
g41=geomcoerce('point',parr);
parr={point2(0.0010,-0.0015+pos)};
g42=geomcoerce('point',parr);
parr={point2(0.0020,-0.0015+pos)};
g43=geomcoerce('point',parr);
parr={point2(0,-0.0025+pos)};
g44=geomcoerce('point',parr);
parr={point2(0.0010,-0.0025+pos)};
g45=geomcoerce('point',parr);
parr={point2(0.0020,-0.0025+pos)};
g46=geomcoerce('point',parr);
parr={point2(0,-0.0035+pos)};
g47=geomcoerce('point',parr);
parr={point2(0.0010,-0.0035+pos)};
g48=geomcoerce('point',parr);
parr={point2(0.0020,-0.0035+pos)};
g49=geomcoerce('point',parr);

%Copies conductors and points for return part of coil
[g74,g75,g76,g77,g78,g79,g80,g81,g82,g83,g84,g85,g86,g87,g88,g89,g90,g91,g92,g93,g94,g95,g96,g97]=geomcopy({g16,g17,g19,g20,g22, ↙
g23,g25,g26,g33,g34,g35,g37,g38,g39,g40,g41,g42,g43,g44,g45,g46,g47,g48,g49});
g74=move(g74,[0,tau_c]);
g75=move(g75,[0,tau_c]);
g76=move(g76,[0,tau_c]);
g77=move(g77,[0,tau_c]);
g78=move(g78,[0,tau_c]);
g79=move(g79,[0,tau_c]);
g80=move(g80,[0,tau_c]);
g81=move(g81,[0,tau_c]);
g82=move(g82,[0,tau_c]);
g83=move(g83,[0,tau_c]);
g84=move(g84,[0,tau_c]);
g85=move(g85,[0,tau_c]);
g86=move(g86,[0,tau_c]);
g87=move(g87,[0,tau_c]);
g88=move(g88,[0,tau_c]);
g89=move(g89,[0,tau_c]);
g90=move(g90,[0,tau_c]);
g91=move(g91,[0,tau_c]);
g92=move(g92,[0,tau_c]);
g93=move(g93,[0,tau_c]);
g94=move(g94,[0,tau_c]);
g95=move(g95,[0,tau_c]);
g96=move(g96,[0,tau_c]);
g97=move(g97,[0,tau_c]);

% Analyzed geometry
clear p s
p.objs={g38,g39,g40,g41,g42,g43,g44,g45,g46,g47,g48,g49,g86,g87,g88, ...
  g89,g90,g91,g92,g93,g94,g95,g96,g97};
p.name={'PT1','PT2','PT3','PT4','PT5','PT6','PT7','PT8','PT9','PT10', ...
  'PT11','PT12','PT13','PT14','PT15','PT16','PT17','PT18','PT19','PT20', ...
  'PT21','PT22','PT23','PT24'};
p.tags={'g38','g39','g40','g41','g42','g43','g44','g45','g46','g47', ...
  'g48','g49','g86','g87','g88','g89','g90','g91','g92','g93','g94','g95', ...
  'g96','g97'};

s.objs={g1,g2,g3,g4,g5,g6,g16,g17,g19,g20,g22,g23,g25,g26,g33,g34, ...
  g35,g37,g74,g75,g76,g77,g78,g79,g80,g81,g82,g83,g84,g85};
s.name={'R1','R2','R3','R4','R5','R6','C2','C3','C5','C6','C8','C9', ...
  'C11','C12','CO1','CO2','CO3','CO5','C1','C4','C7','C10','C13','C14', ...
```

```matlab
  'C15','C16','CO4','CO6','CO7','CO8'};
s.tags={'g1','g2','g3','g4','g5','g6','g16','g17','g19','g20','g22', ...
  'g23','g25','g26','g33','g34','g35','g37','g74','g75','g76','g77','g78', ...
  'g79','g80','g81','g82','g83','g84','g85'};

fem.draw=struct('p',p,'s',s);
fem.geom=geomcsg(fem);

% Initialize mesh
fem.mesh=meshinit(fem, ...
          'hauto',9);


% (Default values are not included)

% Application mode 1
clear appl
appl.mode.class = 'FlPerpendicularCurrents';
appl.assignsuffix = '_qa';
clear bnd
bnd.type = {'A0','cont','tH0'};
bnd.ind = [3,3,3,3,3,3,3,3,3,3,3,3,3,3,3,3,3,3,3,3,3,2,2,2,2,2,2,2,2,2, ...
  2,2,2,2,3,2,2,2,2,2,2,2,2,3,1,2,2,2,2,2,2,2,2,2,2,2,2,2,2,2,2,2,2,2,2, ...
  2,2,2,2,2,2,2,2,2,2,2,2,2,2,2,2,2,2,2,2,2,2,2,2,2,2,2,2,2,2,2,2,2,2,2, ...
  2,2,2,2,2,2,2,2,2,2,2,2,2,2,2,2,2,2,2,2,2,2,2];
appl.bnd = bnd;
clear equ
equ.epsilonr = {1,'mat2_epsilonr',1,1,'mat1_epsilonr'};
equ.magconstrel = {'mur','mur','Br','Br','Br'};
equ.Br = {{0;0},{0;0},{-1.15;0},{1.15;0},{0;0}};
equ.sigma = {0,'mat2_sigma',0,0,'mat1_sigma'};
equ.mur = {1,'mat2_mur',1.035,1.035,'mat1_mur'};
equ.ind = [1,2,2,2,2,2,2,2,2,3,4,3,4,5,1,1,1,1,1,1,2,2,2,2,2,2,2,2,1,1, ...
  1,1,1,1,2,2,2,2,2,2,2];
appl.equ = equ;
fem.appl{1} = appl;
fem.frame = {'ref'};
fem.border = 1;
clear units;
units.basesystem = 'SI';
fem.units = units;

% Library materials
clear lib
lib.mat{1}.name='Iron';
lib.mat{1}.varname='mat1';
lib.mat{1}.variables.sigma='1.12e7[S/m]';
lib.mat{1}.variables.mur='4000';
lib.mat{1}.variables.k='76.2[W/(m*K)]';
lib.mat{1}.variables.epsilonr='1';
lib.mat{1}.variables.rho='7870[kg/m^3]';
lib.mat{1}.variables.C='440[J/(kg*K)]';
lib.mat{1}.variables.nu='0.29';
lib.mat{1}.variables.alpha='12.2e-6[1/K]';
lib.mat{1}.variables.E='200e9[Pa]';
lib.mat{2}.name='Copper';
lib.mat{2}.varname='mat2';
lib.mat{2}.variables.sigma='5.998e7[S/m]';
lib.mat{2}.variables.mur='1';
lib.mat{2}.variables.k='400[W/(m*K)]';
lib.mat{2}.variables.epsilonr='1';
lib.mat{2}.variables.rho='8700[kg/m^3]';
lib.mat{2}.variables.C='385[J/(kg*K)]';
lib.mat{2}.variables.nu='0.35';
lib.mat{2}.variables.alpha='17e-6[1/K]';
lib.mat{2}.variables.E='110e9[Pa]';

fem.lib = lib;

% Multiphysics
fem=multiphysics(fem);
```

```matlab
% Extend mesh
fem.xmesh=meshextend(fem);

% Solve problem
fem.sol=femstatic(fem, ...
            'solcomp',{'Az'}, ...
            'outcomp',{'Az'});

% Save current fem structure for restart purposes
fem0=fem;

% Plot solution
postplot(fem, ...
        'tridata',{'Az','cont','internal','unit','Wb/m'}, ...
        'trimap','jet(1024)', ...
        'contdata',{'normB_qa','cont','internal','unit','T'}, ...
        'contlevels',20, ...
        'contlabel','off', ...
        'contmap','cool(1024)', ...
        'title','Surface: Magnetic potential, z component [Wb/m]   Contour: Magnetic flux density, norm [T]', ...
        'axisequal','off', ...
        'axis',[-0.004593311314017341,0.017022360482446798,-0.04103291143664484,0.04224916768292683,-1,1]);

%Magnetic potential for turn conductors
% Integrate
I1=postint(fem,'Az', ...
        'unit','Wb/m', ...
        'dl',[9], ...
        'edim',0);

% Integrate
I2=postint(fem,'Az', ...
        'unit','Wb/m', ...
        'dl',[36], ...
        'edim',0);

% Integrate
I3=postint(fem,'Az', ...
        'unit','Wb/m', ...
        'dl',[62], ...
        'edim',0);

% Integrate
I4=postint(fem,'Az', ...
        'unit','Wb/m', ...
        'dl',[7], ...
        'edim',0);

% Integrate
I5=postint(fem,'Az', ...
        'unit','Wb/m', ...
        'dl',[34], ...
        'edim',0);

% Integrate
I6=postint(fem,'Az', ...
        'unit','Wb/m', ...
        'dl',[60], ...
        'edim',0);

% Integrate
I7=postint(fem,'Az', ...
        'unit','Wb/m', ...
        'dl',[5], ...
        'edim',0);

% Integrate
I8=postint(fem,'Az', ...
        'unit','Wb/m', ...
        'dl',[32], ...
        'edim',0);
```

```matlab
% Integrate
I9=postint(fem,'Az', ...
        'unit','Wb/m', ...
        'dl',[58], ...
        'edim',0);

% Integrate
I10=postint(fem,'Az', ...
        'unit','Wb/m', ...
        'dl',[3], ...
        'edim',0);

% Integrate
I11=postint(fem,'Az', ...
        'unit','Wb/m', ...
        'dl',[30], ...
        'edim',0);

% Integrate
I12=postint(fem,'Az', ...
        'unit','Wb/m', ...
        'dl',[56], ...
        'edim',0);

%Magnetic potential for return conductors
% Integrate
I13=postint(fem,'Az', ...
        'unit','Wb/m', ...
        'dl',[12], ...
        'edim',0);

% Integrate
I14=postint(fem,'Az', ...
        'unit','Wb/m', ...
        'dl',[39], ...
        'edim',0);

% Integrate
I15=postint(fem,'Az', ...
        'unit','Wb/m', ...
        'dl',[65], ...
        'edim',0);

% Integrate
I16=postint(fem,'Az', ...
        'unit','Wb/m', ...
        'dl',[14], ...
        'edim',0);

% Integrate
I17=postint(fem,'Az', ...
        'unit','Wb/m', ...
        'dl',[41], ...
        'edim',0);

% Integrate
I18=postint(fem,'Az', ...
        'unit','Wb/m', ...
        'dl',[67], ...
        'edim',0);

% Integrate
I19=postint(fem,'Az', ...
        'unit','Wb/m', ...
        'dl',[16], ...
        'edim',0);

% Integrate
I20=postint(fem,'Az', ...
        'unit','Wb/m', ...
        'dl',[43], ...
        'edim',0);
```

```matlab
% Integrate
I21=postint(fem,'Az', ...
        'unit','Wb/m', ...
        'dl',[69], ...
        'edim',0);

% Integrate
I22=postint(fem,'Az', ...
        'unit','Wb/m', ...
        'dl',[18], ...
        'edim',0);

% Integrate
I23=postint(fem,'Az', ...
        'unit','Wb/m', ...
        'dl',[45], ...
        'edim',0);

% Integrate
I24=postint(fem,'Az', ...
        'unit','Wb/m', ...
        'dl',[71], ...
        'edim',0);

flux(1,i) = I9-I21;
flux(2,i) = I5-I17;
flux(3,i) = I1-I13;
flux(4,i) = flux(2,i);
flux(5,i) = flux(1,i);
flux(6,i) = I10-I22;
flux(7,i) = I6-I16;
flux(8,i) = I2-I14;
flux(9,i) = flux(7,i);
flux(10,i) = flux(6,i);
flux(11,i) = I11-I23;
flux(12,i) = I7-I19;
flux(13,i) = I3-I15;
flux(14,i) = flux(12,i);
flux(15,i) = flux(11,i);
flux(16,i) = I12-I24;
flux(17,i) = I8-I20;
flux(18,i) = I4-I16;
flux(19,i) = flux(17,i);
flux(20,i) = flux(16,i);

position(i) = pos;

end

for turn = 1:1:20
    flux(turn,i+1)=flux(turn,2);
end

timeflux = linspace(0, 2/el_freq, 4*i-4) -0.5/el_freq/(i-1);

for vikl = 1:1:20
    dPhi_dt(vikl,1:(i-1))= diff(flux(vikl,1:i))./diff(timeflux(1:i));
end

for j = 1:1:i-1
    v_vikl(j) = sum(dPhi_dt(1:20,j));
end

indusertspenning(tellerting,1:j)=v_vikl;

timevolt(1:4*j-1) = timeflux(1:4*j-1) - timeflux(1);

if q == 1
    totalvoltage(1,1:j) = v_vikl*55;
    totalvoltage(1,i:2*j)=-totalvoltage(1,1:j);
    totalvoltage(1,2*j+1:4*j)= totalvoltage(1,1:2*j);
```

```matlab
elseif q == 12/11
   voltage_v_12_11(1,1:(j)) = v_vikl;
    for k = 2:1:12
      voltage_v_12_11(k,1:j*(k-1)*5/360) = -v_vikl((j+1-(k-1)*5*j/360):j);
      voltage_v_12_11(k,(j*(k-1)*5/360+1):j) = v_vikl(1:j-(k-1)*5*j/360);
    end
   totalvoltage(2,1:j) = sum(voltage_v_12_11)*55/k*q;
   totalvoltage(2,i:2*j)= -totalvoltage(2,1:j);
   totalvoltage(2,2*j+1:4*j)= totalvoltage(2,1:2*j);

elseif q == 6/5
   voltage_v_6_5(1,1:j) = v_vikl;
    for k = 2:1:6
      voltage_v_6_5(k,1:j*(k-1)*10/360) = -v_vikl((j+1-(k-1)*10*j/360):j);
      voltage_v_6_5(k,(j*(k-1)*10/360+1):j) = v_vikl(1:j-(k-1)*10*j/360);
    end
   totalvoltage(3,1:j) = sum(voltage_v_6_5)*55/k*q;
   totalvoltage(3,j+1:2*j)= -totalvoltage(3,1:j);
   totalvoltage(3,2*j+1:4*j)= totalvoltage(3,1:2*j);
end

end

plot(timevolt, totalvoltage(1,1:4*j), timevolt, totalvoltage(2,1:4*j), timevolt, totalvoltage(3,1:4*j))
```

APPENDIX 4: MEASUREMENTS FOR MUTUAL INDUCTANCE

Measurements for mutual inductance

Frequency = 50 Hz

Current [A, RMS]	Induced voltage [mV, p-p]	Induced voltage [mV, RMS]	Mutual inductance [uH]
Test 1			
7.89 R	344 S	121.6224	49.066669
7.76 R	320 T	113.1371	46.408058
8.19 S	348 R	123.0366	47.818998
8.07 S	355 T	125.5115	49.506241
7.85 T	324 R	114.5513	46.449441
8.65 T	383 S	135.4109	49.829646
Test 2			
8.15 R	350 S	123.7437	48.329864
8.09 R	346 T	122.3295	48.131867
8.35 S	366 R	129.4005	49.328708
8.14 S	358 T	126.5721	49.495277
8.1 T	334 R	118.0868	46.405193
7.92 T	346 S	122.3295	49.165001
Test 3			
8.25 R	350 S	123.7437	47.744047
8.25 R	346 T	122.3295	47.198401
8.54 S	376 R	132.9361	49.549024
8.4 S	378 T	133.6432	50.642793
8.02 T	344 R	121.6224	48.271324
8.29 T	362 S	127.9863	49.142718

	Standard deviation [uH]	Mean values [uH]
RS	0.781748	48.639552
RT	0.874021	47.144047
ST	0.557269	49.630279